Title: **PPARα-NFκB heterodimer mediates obesity-induced diastolic dysfunction through autocrine production of IL-6**

Shin-ichi Oka[1], Eun-Ah Sung[1], Peiyong Zhai[1], Kevin Schesing[1], Santosh Bhat[1], Adave Chin[1], Jiyeon Park[2], Yeun-Jun Chung[2], Akihiro Shirakabe[1], Takanobu Yamamoto[1], Yoshiyuki Ikeda[1], Wataru Mizushima[1], Shohei Ikeda[1], Mingming Tong[1], Jaemin Byun[1], Michinari Nakamura[1], Samuel Kim[1], Jamie Francisco[1], Dominic P Del Re[1] and Junichi Sadoshima[1]

Affiliation:

[1]Rutgers New Jersey Medical School Department of Cell Biology and Molecular Medicine, Rutgers Biomedical and Health Sciences, Newark, NJ 07101.

[2]Precision Medicine Research Center, College of Medicine, The Catholic University of Korea, Seoul, Republic of Korea.

Running Title: PPAR-induced IL-6 mediates diastolic dysfunction in obesity

Correspondence:
Junichi Sadoshima, MD PhD
Cardiovascular Research Institute,
Rutgers Biomedical and Health Science
185 South Orange Ave., MSB G609
Newark, NJ 07103
Tel: (973)972-8619
Fax: (973)972-8919
Email: sadoshju@njms.rutgers.edu

SUMMARY

Obesity is accompanied by increases in free fatty acids (FFAs) in the systemic circulation, and obese patients often develop cardiac hypertrophy and diastolic dysfunction, termed obesity cardiomyopathy. Proinflammatory cytokines, including IL-6, have been implicated in the pathogenesis of the cardiac dysfunction associated with obesity cardiomyopathy. Elevation of FFAs induced by high fat diet (HFD) consumption induced diastolic dysfunction in the heart as early as after one month. HFD consumption directly stimulated IL-6 production in cardiomyocytes before local inflammation developed and induced diastolic dysfunction even in the presence of macrophage depletion with clodronate in the heart. PPARα played an essential role in mediating *Il6* transcription in response to HFD consumption by forming a heterodimer with p50/RelA and binding to the NFκB element in cardiomyocytes. Local production of IL-6 in cardiomyocytes, in turn, mediated the development of diastolic cardiac dysfunction. HFD-induced diastolic dysfunction was attenuated by cardiac-specific deletion of either *Ppara* or *Il6*, as well as by interference with the PPARα-NFκB heterodimer formation by a molecular decoy. These results suggest that elevated FFAs directly upregulate *Il6* through the PPARα-NFκB heterodimer in cardiomyocytes and highlight autocrine production of IL-6 as a key downstream mechanism in the initial development of diastolic dysfunction.

Keywords: PPARα, NFκB, IL-6, diastolic dysfunction

INTRODUCTION

The prevalence of obesity, a major risk factor for type II diabetes, is increasing rapidly worldwide (1). More than half of obese patients develop myocardial dysfunction, known as obesity cardiomyopathy (2). In its early phase, diastolic dysfunction, left ventricular (LV) hypertrophy, and fibrosis are observed. Some patients develop heart failure with preserved ejection fraction (HFpEF), while others develop heart failure with reduced ejection fraction (HFrEF) (3). Currently, there is no effective medical treatment for obesity cardiomyopathy and HFpEF (4).

The hearts of patients with obesity, insulin resistance, type II diabetes, and HFpEF often develop low grade inflammation (5, 6). Pro-inflammatory cytokines and chemokines, including TNF-α, IL-1β, IL-6, and MCP-1, play an essential role in mediating the development of obesity cardiomyopathy (7, 8). Among the cytokines, IL-6 has been frequently associated with insulin resistance, diastolic dysfunction, fibrosis and other features of obesity cardiomyopathy in humans (9) and experimental animals fed a high fat diet (HFD) (10), (11). IL-6 acts by binding to soluble IL-6 receptors and gp130, stimulating a trans signaling response (10) and promoting cardiac fibrosis, hypertrophy, and stiffening through multiple mechanisms, including de-phosphorylation of titin in cardiomyocytes (12). Importantly, however, *which cell type* produces the cytokines during the initial phase of obesity cardiomyopathy and *how their production is induced* are poorly understood.

Nuclear factor kappa-light-chain-enhancer of activated B cells (NFκB) is a transcription factor composed of Rel and p50 proteins. NFκB plays a central role in immune and inflammatory reactions. Although free fatty acid (FFA) activates the proinflammatory NFκB pathway in the liver (13), the precise mechanism connecting FFA and NFκB is not well understood. Importantly, many patients with mild obesity have either mild or even no obvious inflammation in the heart. It is important to elucidate how inflammation is initiated in the heart in these conditions.

PPARα is a nuclear receptor involved in fatty acid oxidation (FAO) (14-17). The activity of PPARα is regulated by FFA ligands, PGC-1s, transcription (18), and posttranslational modification (17). PPARα is critically involved in the pathogenesis of obesity cardiomyopathy (19), and overexpression of PPARα in the heart induces lipotoxicity and obesity cardiomyopathy (20). Downregulation of PPARα in *systemic Ppara* knockout (KO) mice is generally protective against obesity cardiomyopathy (20-22). These observations suggest that PPARα is a therapeutic target for obesity cardiomyopathy. However, *whether PPARα inhibits or stimulates inflammation, an important mechanism facilitating the progression of obesity cardiomyopathy, has been controversial* (23-26).

Since obesity is a condition in which fatty acid ligands are enriched in the body and induce low-grade inflammation (27), we reasoned that PPARα may mediate obesity-induced low-grade inflammation. We here propose that PPARα induces *Il6* in cardiomyocytes in obesity, through physical interaction with NFκB. We asked 1) whether upregulation of IL-6 in cardiomyocytes through a PPARα-dependent mechanism plays an important role in mediating the diastolic dysfunction in response to HFD consumption, and 2) whether heterodimerization between PPARα and an NFκB subunit, and binding of the heterodimer to the κB element play an essential role in mediating IL-6 production. Our study provides mechanistic information about how obesity initiates local production of IL-6, which in turn leads to diastolic dysfunction.

Results

PPARα is activated during the development of diastolic dysfunction

To induce diastolic dysfunction, we fed mice a HFD (60 kcal%), an established method of inducing obesity cardiomyopathy (28) (**Fig. S1A**). After 1 to 3 months of HFD consumption, diastolic dysfunction was assessed by performing pressure-volume (PV) loop analyses. The PV loop analysis continuously measures left ventricular (LV) pressure and volume in the beating

heart (**Fig. S1B**). Diastolic dysfunction is characterized by elevated LV blood pressure at end-diastole. We used end diastolic pressure (EDP) and EDP-volume relationship (EDPVR) as indices of diastolic function (29). Diastolic dysfunction, characterized by increased EDP and EDPVR, was observed as early as after 1 month of HFD consumption and remained significant at 3 months in wild type (WT) mice (**Fig. S1C**). Both male and female mice exhibited similar trends, and no significant sex-based differences were observed in either EDP or EDPVR measurements (**Fig. S1C**). Among genes known to be involved in diastolic dysfunction, *Atp2a2* was downregulated, while *Myh7* was upregulated after 1 month of HFD consumption (Fig. S1D). *Mmp2* showed a trend toward upregulation, whereas *Col1a1* expression was not significantly changed (**Fig. S1D**). *Atp2a2* contributes to myocardial relaxation via calcium reuptake, and its downregulation may contribute to diastolic dysfunction (30). *Myh7*, a fetal isoform of β-myosin heavy chain, is re-expressed under pathological conditions and is associated with impaired contractile and relaxation properties (31). *Mmp2* and *Col1a1* are involved in fibrosis (32), and their limited induction after 1 month of HFD is consistent with the absence of overt myocardial fibrosis at this early time point (Fig. 2E, right panel). Cardiac systolic function, evaluated via the end systolic pressure-volume relationship (ESPVR) and the echocardiographically determined LV ejection fraction (LVEF), was preserved under HFD consumption conditions (**Fig. S1E**). LV end diastolic dimension (LVEDD) was increased after two months and LV end systolic dimension (LVESD) was increased after three months of HFD consumption (**Fig. S1F**), whereas LVEF was not altered at these time points. These results are consistent with the presence of volume overload during HFD consumption. It should be noted that both diastolic dysfunction and RNA expression of genes involved in diastolic/cardiac dysfunction were observed as early as one month of HFD consumption. Thus, elevation of LVEDP is caused by diastolic dysfunction and not merely by volume overload.

Since FFAs act as ligands for PPARα, increased plasma FFAs resulting from HFD consumption may activate PPARα. To investigate whether HFD activates PPARα in

cardiomyocytes, we used *Ribo-tag* mice, transgenic mice with Cre driver-dependent expression of HA-tagged Rpl22, a ribosomal protein, and evaluated whether known targets of PPARα are upregulated in response to HFD consumption. In this system, by crossing *Ribo-tag* mice with *Myh6*-Cre (*Ribo-tag*: *Myh6-Cre*) mice, HA-Rpl22 is expressed only in cardiomyocytes, such that immunoprecipitation with anti-HA antibody selectively pulls down ribosome-associated mRNA from cardiomyocytes. As shown in **Fig. 1A**, after immunoprecipitation with anti-HA antibody, *β-actin* (*Actb*) mRNA was significantly enriched in heart samples from *Ribo-tag*: *Myh6*-Cre mice compared to in those from *Ribo-tag* mice, confirming Cre-dependent expression of HA-Rpl22 and successful isolation of cardiomyocyte-specific mRNA. The expression of PPARα target genes, including *Acox1, Cd36, Cpt1b* and *Pdk4*, was significantly upregulated in cardiomyocytes in *Ribo-tag*: *Myh6*-Cre mice in response to HFD consumption, suggesting that HFD consumption upregulates PPARα targets in cardiomyocytes (**Fig. 1B**).

To investigate whether PPARα directly regulates the target genes identified above, chromatin immunoprecipitation sequencing (ChIP-seq) with anti-PPARα antibody was performed. PPARα was localized near the PPAR response element (PPRE) in the promoters of known PPARα target genes such as *Acox1, Cd36, Cpt1b, Ech1, Fatp1* and *Pdk4*. Recruitment of PPARα to near PPREs appeared to be enhanced at the *Acox1, Cd36, Cpt1b* and *Pdk4* promoters, but not at the *Ech1* or *Fatp1* (*Slc27a1*) promoters, in response to HFD consumption (**Fig. 1C**). These results are consistent with the notion that induction of PPARα target genes occurs with or without a detectable increase in PPARα recruitment to promoters. The latter mechanism involves a ligand-dependent switch in PPARα binding partners, from transcriptional repressors to co-activators, rather than increased promoter occupancy.

To further evaluate the role of PPARα in mediating upregulation of PPARα target genes during HFD consumption, we fed cardiac-specific *Ppara* knockout (*Ppara* cKO) and overexpression (Tg-*Ppara*) mice either HFD or ND. The HFD-induced upregulation of PPARα

target genes was inhibited in *Ppara* cKO mice **(Fig. 1D)**. Suppression of PPARα target gene expression was also observed in systemic *Ppara* knockout (*Ppara* KO) mice (**Fig. S2A**). On the other hand, the expression of *Acox1, Cpt1b* and *Ech1* was significantly enhanced and that of *Cd36, Fatp1* and *Pdk4* exhibited a trend of enhancement in Tg-*Ppara* mice. Together, these results suggest that PPARα is activated in response to HFD consumption and contributes to changes in gene expression during the development of HFD-induced diastolic heart dysfunction.

PPARα plays an essential role in mediating diastolic dysfunction in response to HFD consumption

To investigate the role of PPARα in mediating HFD-induced diastolic dysfunction, *Ppara* cKO and Tg-*Ppara* mice were fed a HFD for 1 month. Diastolic dysfunction, as evidenced by increased EDP and EDPVR, was ameliorated in *Ppara* cKO but exacerbated in Tg-*Ppara* mice compared to in respective WT mice (**Fig. 2A**). LVEF was comparable between *Ppara* cKO and WT mice after both ND and HFD consumption (**Fig. 2B**). Overexpression of *Ppara* alone promotes metabolic derangement, which is enhanced by HFD consumption due to increased ligand binding to PPARα (20, 33). As reported previously (33, 34), Tg-*Ppara* mice exhibited systolic dysfunction during ND consumption, and this was exacerbated during HFD consumption (**Fig. 2AB**). *Ppara* cKO mice did not show lung congestion, as assessed by the lung weight-to-tibia length ratio, nor did they develop cardiac hypertrophy, as evaluated by the heart weight-to-tibia length ratio (**Figs. 2CD)**. In contrast, *Tg-Ppara* mice displayed significant lung congestion and cardiac hypertrophy under HFD conditions, consistent with previous reports (20, 33). Cardiac fibrosis was observed after 3 months of HFD consumption in WT mice but was not significant in *Ppara* cKO mice **(Fig. 2E**). Because Tg-*Ppara* mice fed HFD exhibited a high mortality rate (data not shown), cardiac fibrosis was examined after only one month of HFD consumption. Although cardiac fibrosis was not observed at this time point in WT mice, there

was significant fibrosis in Tg-*Ppara* mice after both ND and HFD consumption. Systemic *Ppara* KO mice exhibited similar outcomes to those of *Ppara* cKO mice (**Fig. S2B-F**). These results suggest that PPARα in cardiomyocytes plays an essential role in the development of HFD-induced diastolic dysfunction. To test whether PPARα continues to contribute to diastolic dysfunction during prolonged HFD exposure, *Ppara* cKO mice were fed HFD for 4 months (**Fig. 2F**). HFD-induced increases in EDP and EDPVR remained inhibited in *Ppara* cKO mice, suggesting that cardiomyocyte PPARα continues to mediate diastolic dysfunction during extended metabolic stress. However, *Ppara* cKO mice exhibited a trend toward reduced LVEF and increased lung weight and cardiac hypertrophy was enhanced in *Ppara* cKO mice compared to in WT controls. These findings suggest that while *Ppara* deletion protects against diastolic abnormalities, it may impair the metabolic adaptation of the heart during sustained lipid overload.

PPARα mediates HFD-induced IL-6 production in cardiomyocytes, thereby promoting diastolic dysfunction

The low-grade inflammation induced by obesity is thought to promote diastolic dysfunction (35). Cardiomyocytes produce inflammatory cytokines, including tumor necrosis factor-α (TNFα) and IL-6 (36). To assess whether PPARα modulates immune and inflammatory gene expression, we conducted RNA sequencing of H9c2 cardiomyoblasts in the presence or absence of *Ppara* overexpression. Among the inflammatory genes categorized under the Gene Ontology Biological Process (GOBP) "Regulation of Response to Cytokine Stimulus," more genes were upregulated than suppressed by *Ppara* overexpression, with upregulated genes including *Cas1*, *Tlr4*, *Il6*, and *Ripk2*, suggesting that PPARα activates these immune and inflammatory genes in a cell-autonomous manner **(Fig. 3A**). We next examined the role of PPARα in mediating HFD-induced inflammatory cytokine expression in the heart. Since diastolic dysfunction was

observed within one month of HFD consumption, we fed mice ND or HFD for one month. We examined four major inflammatory cytokines, *Il1a*, *Il1b*, *Il6*, and *Tnfa*, which have been reported to be upregulated in obesity (37). As shown in **Fig. 3B**, cytokine expression tended to increase in response to HFD consumption, an effect that was attenuated in *Ppara* cKO but enhanced in Tg-*Ppara* mice. Systemic *Ppara* KO mice exhibited similar outcomes to those of *Ppara* cKO mice (**Fig. S2G**). *Il1a* expression was not detectable in any of the mice, suggesting that IL-1α may be silenced in the heart. The HFD-induced cytokine expression in the heart could play a role in immune cell infiltration. However, FACS analyses revealed no significant changes in leukocytes, macrophages, monocytes, neutrophils or T-cells in the heart in response to HFD consumption for one month compared to in response to pressure overload, which served as a positive control for our analyses (**Fig. S3A**). As shown in **Fig. S3B**, CD68, a macrophage marker, was also not significantly affected by HFD consumption in WT, *Ppara* KO or *Ppara* cKO mice. However, a trend toward an increase in CD68 was observed in Tg-*Ppara* mice fed HFD. These results suggest that WT mice develop diastolic dysfunction after one month of HFD consumption, even before histological manifestation of inflammatory cell infiltration. To investigate the role of macrophages in diastolic dysfunction, these cell types were depleted with clodronate (38) (**Fig. S3C**). Macrophage depletion did not inhibit HFD-induced diastolic dysfunction, suggesting that macrophages do not play a major role in mediating diastolic dysfunction in response to HFD consumption (**Fig. S3D**).

Among the cytokines we tested, *Il6* was one of the most prominently upregulated during HFD consumption, and its upregulation was PPARα-dependent in the heart (**Fig. 3A and 3B**). We confirmed the statistical significance in analyses of male/female mice combined and male mice alone, but not in female mice alone due to the insufficient availability of mice (**Fig. S3E**). HFD-induced *Il6* upregulation in cardiomyocytes was verified with *Ribo-tag*: *Myh6*-Cre mice (**Fig. 3C**). Upregulation of *Il6* mRNA in response to HFD consumption was inhibited in adult

cardiomyocytes isolated from *Ppara* cKO mice (**Fig. 3D**). Thus, HFD induces *Il6* in cardiomyocytes in a PPARα-dependent manner. To further investigate the cellular source of IL-6 within the heart, cardiac tissue was fractionated into cardiomyocyte and non-cardiomyocyte fractions. IL-6 expression was significantly induced in cardiomyocytes, whereas only a modest increase was observed in non-cardiomyocytes (**Fig. S3F**), supporting that cardiomyocytes are the primary contributors to IL-6 production in response to HFD consumption.

To investigate whether PPARα mediates systemic IL-6 induction in response to HFD consumption, the IL-6 level in the plasma was evaluated. HFD increased the plasma level of IL-6, an effect that was completely inhibited in *Ppara* KO mice (**Fig. 3E**). However, HFD-induced increases in the plasma IL-6 level were not significantly altered in *Ppara* cKO or Tg-*Ppara* mice (**Fig. 3E**). Thus, PPARα in cardiomyocytes does not contribute to the increased level of plasma IL-6 in response to HFD consumption. Furthermore, diastolic dysfunction was associated with the IL-6 level in cardiomyocytes, rather than that in the plasma, in *Ppara* cKO and Tg-*Ppara* mice.

To investigate whether IL-6 produced by cardiomyocytes contributes to diastolic dysfunction, cardiac-specific *Il6* knockout (*Il6* cKO) mice were generated. *Il6* cKO mice did not show any sign of cardiac hypertrophy or lung congestion at baseline (**Table S1**). The IL-6 level in the heart, evaluated with immunoblot analyses, was significantly elevated in response to one month of HFD consumption in WT mice (**Fig. 3F**). However, it was significantly lower in *Il6* cKO mice both at baseline and in response to HFD consumption, suggesting that cardiomyocytes are the major cell type in which IL-6 is produced at baseline and upregulated after one month of HFD consumption. HFD-induced diastolic dysfunction was completely prevented in *Il6* cKO mice, suggesting that IL-6 produced by cardiomyocytes plays a key role in diastolic dysfunction development (**Fig. 3G**). Taken together, these results suggest that PPARα in cardiomyocytes contributes to diastolic dysfunction through local production of IL-6 in cardiomyocytes. We also

used anti-IL-6R antibody to block IL-6 signaling. Although a control antibody did not affect the development of diastolic dysfunction in response to HFD consumption, anti-IL-6R antibody fully ameliorated it (**Fig. 3H**). Thus, IL-6 signaling appears to be a promising target for the treatment of diastolic dysfunction associated with obesity.

To investigate downstream signaling events of IL-6, we assessed IL-6Rα levels and phosphorylation of Stat3 at Y705 in the heart (39). Among the downstream mediators of IL-6 signaling, Stat3 is a key effector that not only drives transcription but also interacts cooperatively with other inflammatory regulators, including NFκB, AP-1, and HIF-1α, thereby amplifying inflammatory signaling cascades (40). While IL-6Rα expression was not significantly changed, Stat3 phosphorylation was significantly increased in WT mice after HFD consumption and was attenuated in *Ppara* cKO but enhanced in Tg-*Ppara* mice (**Fig. S3G** and **S3H**). These results suggest that HFD activates Stat3 in a PPARα-dependent manner, independent of changes in IL-6Rα expression.

High IL-6 levels suppress PPARα expression in hepatocytes through Stat1/3 signaling (41). Although HFD-fed mice showed IL-6-dependent Stat3 phosphorylation, cardiac PPARα expression was unchanged in either HFD-fed or *Il6* cKO mice (**Fig. S3I**). These results suggest that IL-6 promotes diastolic dysfunction in the heart through activation of Stat3 signaling, rather than through suppression of PPARα.

Gain of PPARα function promotes lipotoxicity, characterized by increased myocardial triglyceride content, and contributes to cardiac dysfunction (33). To assess the role of endogenous PPARα in this process, we measured myocardial triglyceride levels in *Ppara* KO mice. The HFD-induced increase in triglyceride content was significantly attenuated in *Ppara* KO mice, indicating that lipotoxicity under HFD conditions is PPARα-dependent (**Fig. S3J**). To determine whether IL-6 mediates this lipotoxic response, we measured myocardial triglyceride content in *Il6* cKO mice. In contrast to *Ppara* KO mice, *Il6* cKO mice did not show significant

differences in triglyceride accumulation following HFD feeding (**Fig. S3K**), suggesting that IL-6 does not contribute to lipid accumulation. Taken together, these results indicate that IL-6 mediates only a subset of PPARα-dependent cardiac pathologies, such as diastolic dysfunction, but not lipotoxicity.

Verification of *Il6* induction in cardiomyocytes via single cell RNA sequencing

To further verify that a HFD induces PPARα target gene expression and *Il6* upregulation in cardiomyocytes, single-cell RNA sequencing (scRNA-seq) was performed using mouse heart tissues. In this experiment, cardiomyocytes comprised the majority of sequenced cells. Compared to mice fed a ND, only a limited population of cardiomyocytes was recovered from HFD-fed mice (**Fig. S4A**). This reduction likely indicates increased fragility of cardiomyocytes in mice consuming a HFD, resulting in lower recovery rates during the cell labeling process. This may compromise the analysis of various cardiomyocyte clusters in the context of HFD consumption. In addition, during barcoding and library preparation, cells with elevated mitochondrial RNA content, a marker of cellular stress (42), were excluded during quality control filtering.

Despite this limitation, the analysis of cardiomyocyte clusters confirmed upregulation of PPARα target genes, including *Acox1*, *Cpt1b*, *Cd36*, *Ech1*, and *Acadm*, in cardiomyocytes following HFD consumption (**Fig. S4B**). Consistent with the presence of low-grade inflammation associated with obesity, a modest increase in *Il6* expression was also observed in cardiomyocytes from HFD-fed mice (**Fig. S4C**). In contrast, the expression patterns of *Il-1b*, *Tnf*, and *Mif* differed between qPCR of the whole heart (**Fig. 3B**) and scRNA-seq of cardiomyocyte clusters (**Fig. S4C**), possibly due to differences in the specific cell populations analyzed by each method. A KEGG pathway analysis revealed that HFD consumption stimulated several inflammatory signaling pathways, including primary immunodeficiency, T cell receptor signaling, and NFκB signaling **(Fig. S4D**). Bioinformatics analyses also showed activation of the JAK-

STAT pathway, a downstream signaling pathway activated by IL-6. Collectively, these data confirmed activation of an inflammatory signature and enhanced PPARα and IL-6 signaling in cardiomyocytes in response to HFD consumption.

PPARα mediates fatty acid-induced *Il6* production

To gain insight into how PPARα induces *Il6* in response to HFD consumption, we inspected PPARα binding sequences in the mouse *Il6* promoter. Although the authentic PPRE/DR1 type of PPARα/RXR heterodimer binding sequence was not found, three potential monomeric PPARα binding sequences were identified in the *Il6* promoter (**Fig. 4AB)**. Two of them were aligned with a 3-nucleotide spacer, designated as direct repeat 3 (DR3). The third PPARα binding sequence overlapped with a half site of the NFκB binding sequence to which a monomeric NFκB subunit, such as RelA or p50, can bind, designated as the κB element. To evaluate PPARα binding to the DR3 and the κB element, *in vitro* DNA binding assays were performed with recombinant PPARα and biotin-labeled DNA comprising wild type and mutated versions of the κB element and PPRE, as shown in **Fig. 4BC**. The purity of the recombinant proteins used in this study, including PPARα, RXRα, RelA and p50, is shown in **Fig. S5A.** The DNA binding assay showed that PPARα binds to both the DR3 and the κB element (**Fig. 4D**). PPARα binding to the κB (*Il6* (κB)) element was weaker than to the DR3 but was further reduced when a single-nucleotide mutation (*Il6*m1) was introduced into the κB element, indicating sequence-dependent interaction (**Fig. 4D**).

To test whether PPARα mediates fatty acid-induced *Il6* upregulation in cultured cardiomyocytes, PPARα was knocked down with siRNA. Palmitic acid (PA), a fatty acid, upregulated *Il6* mRNA , an effect that was inhibited by PPARα knockdown (**Fig. 4E and S5B**). Thus, PPARα mediates fatty acid-induced *Il6* transcription in cardiomyocytes.

Because PPARα strongly binds to the DR3, we originally hypothesized that the DR3 mediates PPARα-mediated *Il6* promoter activation. However, both fatty acid ligands, such as PA, oleic acid (OA), and an artificial ligand WY14643 (WY), and overexpression of PPARα activated transcription of a reporter gene harboring the 0.6 Kb *Il6* promoter without the DR3 (**Fig. 4F**). Thus, the DR3 is not necessary for PPARα-induced *Il6* promoter activation. To test whether PPARα mediates fatty acid-induced activation of the *Il6* promoter, the effect of PPARαΔAF2, a dominant negative mutant of PPARα(43), was examined. PA- and OA-induced *Il6* promoter activation was inhibited by PPARαΔAF2 (**Fig. 4G**). We also exogenously expressed *Ppara* in Cos7 cells to further examine the role of PPARα in *Il6* induction. PA and WY significantly activated the *Il6* promoter in the presence of exogenous PPARα (**Fig. 4H**).

To test whether PPARα binds to the *Il6* promoter in the heart *in vivo*, chromatin immunoprecipitation assays were performed. PPARα bound to a flanking region of the κB element on the *Il6* promoter under both ND and HFD consumption conditions (**Fig. 4I**). To test whether PPARα binds to the κB element with an affinity equivalent to that for endogenous PPREs, the effect of PPARα dosage upon binding to the κB element was evaluated via pull-down assays with biotin-labeled oligonucleotides harboring endogenous PPRE sequences derived from the *Cd36* and *Acox1* promoters. The binding affinity of PPARα for the κB element was slightly stronger than for the PPRE derived from the *Cd36* promoter and weaker than for the PPRE derived from the *Acox1* promoter, suggesting that the binding affinity of PPARα for the κB element is comparable to that of endogenous PPREs (**Fig. 4J**). These results suggest that PPARα mediates fatty acid-induced *Il6* promoter activation most likely through direct interaction with the κB element.

NFκB mediates fatty acid-induced *Il6* production

Since PPARα binds to the κB element *in vitro*, we next investigated the role of NFκB in mediating PPARα-induced *Il6* promoter activation. To this end, we evaluated the effect of a super-suppressor form of IκBα (IκBαM), which inhibits NFκB. IκBαM inhibited PA-, WY- and *Ppara* overexpression-induced *Il6* promoter activation, suggesting that NFκB is required for PPARα-induced *Il6* induction (**Fig. 4K**). In Tg-*Ppara* mice expressing Flag-tagged PPARα, both RelA and p50 of NFκB were co-immunoprecipitated with Flag-PPARα, suggesting that PPARα binds to NFκB in the heart. The level of interaction between PPARα and RelA/p50 was not altered in HFD consumption (**Fig. S5C**). Proximity ligation assays (PLA) revealed interaction between PPARα and the RelA NFκB subunit in DAPI-positive nuclei in cultured cardiomyocytes (**Fig. 4L**). Recruitment of PPARα and RelA to the *Il6* promoter proximal to the κB element was enhanced in Tg-*Ppara* mice, suggesting that PPARα is capable of recruiting NFκB (**Fig. 4M**). These results suggest that NFκB plays an essential role in PPARα-induced *Il6* transcription, possibly through interaction with PPARα.

PPARα heterodimerizes with NFκB and binds to the κB element

The PPARα binding sequence in the 0.6 Kb region of the *Il6* promoter partially overlaps with the κB element (44). The 5' half of the κB element in the *Il6* promoter possesses a PPARα preferred binding sequence, whereas the 3' half of the κB element represents a typical binding sequence for monomeric Rel or p50 proteins (YYCC; Y: T or C) rather than RXRs (RGKTYA; G:A or G, K: G or T) (**Fig. 4A**). Because direct binding of PPARα to RelA has been reported (45), we hypothesized that PPARα heterodimerizes with either RelA or p50 and binds to the κB element.

To test this hypothesis, *in vitro* protein-protein and protein-DNA binding assays were performed using recombinant proteins and biotin-labeled DNAs. *In vitro* binding assays showed

that PPARα directly binds to p50 as well as to RelA (**Fig. 5A**). *In vitro* competition assays showed that the binding of PPARα to RelA was competitively inhibited by p50, suggesting that both RelA and p50 bind to PPARα in a competitive manner (**Fig. 5B**), such that PPARα can heterodimerize with either RelA or p50. To investigate whether the binding of PPARα to the κB element is promoted by NFκB proteins, DNA binding assays were performed. Binding of PPARα to the κB element was promoted in the presence of either p50 or RelA (**Fig. 5C**). In contrast, binding of p50 or RelA to the κB element was partially reduced by PPARα, but this was not observed when the binding of PPARα to the κB element was inhibited by the introduction of a mutation in the κB element (*Il6* m1) (**Fig. 5C**). This suggests that the reduced binding of p50 and RelA to the κB element in the presence of PPARα is likely due to conversion from p50/p50 or RelA/RelA homodimers to PPARα/p50 or PPARα/RelA heterodimers. Thus, the binding of PPARα to the κB element is promoted by heterodimerization with NFκB proteins, just as binding of PPARα to the PPRE is promoted by heterodimerization with RXR. Through the DNA binding assays, we verified that the binding of PPARα to the endogenous PPREs derived from the *Acox1* and *Cpt1b* promoters was enhanced by RXRα (**Fig. 5D**). Double ChIP assays revealed that PPARα and NFκB were colocalized at the *Il6* promoter (**Fig. 5E**). These results suggest that PPARα heterodimerizes with NFκB, enhancing binding to the κB element.

In order to test whether PPARα binds to other κB elements besides the one in the *Il6* promoter, *in vitro* DNA binding assays were conducted with biotin labeled DNA comprising κB elements from the *Tnfa*, *Mip1b* and *Mip2* promoters (**Fig. 5F and 5G**). PPARα strongly bound to the κB elements derived from the *Il6* and *Tnfa* promoters but not to those from the *Mip2* or *Mip1β* promoters (**Fig. 5G**). To investigate whether the binding of PPARα to these κB elements is enhanced by NFκB, *in vitro* DNA binding assays were performed. Binding of PPARα to the κB element derived from the *Tnfα* promoter was significantly enhanced by p50 (**Fig. 5H**). Although

the binding of PPARα to the κB elements derived from the *Mip2* and *Mip1β* promoters was also enhanced by p50, there was still significantly less PPARα binding to these κB elements than to that from the *Tnfa* promoter. These results suggest that PPARα binds to only a subset of κB elements, and this binding is enhanced by its heterodimerization with NFκB proteins. This subset of κB elements appears to possess a preferred PPARα-binding sequence in its half site, where either authentic NFκB dimer or PPARα/NFκB heterodimer can bind **(Fig. 5I)**.

To evaluate PPARα and NFκB binding to the promoters of inflammatory genes in the heart, ChIP-seq was performed with anti-PPARα, RelA and p50 antibodies. The peaks of PPARα binding were observed in the proximity of the DR3 and κB elements in the *Il6* promoter under ND and HFD feeding conditions (**Fig. 5J**). RelA and p50 were also localized in the proximity of the κB element, but their occupancy declined under HFD feeding conditions. These data suggest that HFD-induced *Il6* expression is not due to increased PPARα–NFκB complex formation, but rather due to a shift in the transcriptional activity of a pre-existing complex caused by ligand binding. We propose that fatty acid ligands activate PPARα within the complex, leading to coactivator recruitment and transcriptional activation, analogous to classical PPARα ligand responses (16, 46), rather than inducing new heterodimerization with NFκB in response to HFD.

As in the oligonucleotide *in vitro* DNA binding assays, PPARα bound to the *Tnfα* promoter but not significantly to the *Mip1β* and *Mip2* promoters (**Fig. 5J**). These results suggest that PPARα transcribes a subset of NFκB target genes via direct binding to their promoters.

PPARα/NFκB heterodimerization is required for fatty acid-induced *Il6* promoter activation

To verify that the binding of PPARα to the κB element is enhanced by heterodimerization with NFκB proteins, we performed *in vitro* DNA binding assays using oligonucleotides harboring the *Il6* promoter with mutated κB elements, namely m2, m3, m4 and m5, and recombinant proteins,

including PPARα, RelA and p50 (**Fig. 6A**). In m5, we mutated the κB element in a way that allows PPARα to bind. This mutant was used as a positive control for PPARα binding and as a negative control for NFκB binding (**Fig. 6B**). In m2, we mutated the PPARα binding region located outside of the NFκB binding region. This mutant can bind an NFκB, but not PPARα, dimer (**Fig. 6B**). Although binding of p50 to the WT κB element was reduced in the presence of PPARα, binding of p50 to m2 was not affected, suggesting that binding of PPARα to the half site of the κB element reduces p50 binding, most likely due to the conversion from p50/p50 homodimers to PPARα/p50 heterodimers (**Fig. 6C**). In m3, we mutated the 3' half site of the κB element to inhibit binding of NFκB without affecting the binding of monomeric PPARα. Although binding of PPARα to the WT κB element was enhanced by p50, binding of PPARα to m3 was not enhanced in the presence of p50 (**Fig. 6D**). These results suggest that the binding of PPARα to the κB element is enhanced when NFκB binds to the 3' half site of the κB element. In m4, in order to inhibit binding of an NFκB dimer but allow binding of a PPARα/NFκB heterodimer, we introduced a point mutation in the 5' half site, which partially reduces the DNA binding of NFκB without affecting PPARα binding (**Fig. 6B**). Although binding of p50 to m4 was reduced in the absence of PPARα, it was not reduced in the presence of PPARα (**Fig. 6E**). Rather, the binding of p50 to m4 was promoted in the presence of PPARα. This suggests that the presence of PPARα supports binding of p50, most likely through formation of the PPARα/p50 heterodimer. Taken together, these results suggest that PPARα heterodimerizes with NFκB and binds to the κB element.

Based upon the results of the experiments shown in **Fig. 6A-E**, how monomeric PPARα, NFκB dimer, and PPARα/NFκB heterodimer bind to these mutants is summarized in **Fig. 6F**. To investigate whether PPARα and NFκB heterodimerization is required for *Il6* promoter activation, reporter gene assays were performed using luciferase reporter genes harboring the 1 Kb *Il6*

promoter with mutations corresponding to either m2, m3 or m4. PA-induced *Il6* promoter activation was abolished when PPARα/NFκB heterodimer binding was inhibited in reporters harboring m2 or m3. In contrast, PA-induced *Il6* promoter activation was not inhibited when NFκB dimer binding was inhibited but PPARα/NFκB heterodimer binding was allowed in the reporter harboring m4 (**Fig. 6G**). These results suggest that PPARα/NFκB heterodimer, rather than authentic NFκB dimer, is required for fatty acid-induced *Il6* promoter activation. In contrast, TNFα-induced *Il6* promoter activation was inhibited when NFκB dimer binding was inhibited in reporters harboring m3 or m4, whereas it was not inhibited when PPARα/NFκB heterodimer binding was inhibited but NFκB dimer binding was allowed in the reporter harboring m2 (**Fig. 6H**). These results suggest that authentic NFκB dimer, rather than PPARα/NFκB heterodimer, is required for TNFα-induced *Il6* promoter activation. In summary, PPARα/NFκB heterodimer is required for fatty acid-induced *Il6* induction through the κB element, whereas PPARα is not essential for *Il6* induction by other stimuli such as TNFα.

Although our results suggest that PPARα cooperatively works with NFκB to activate transcription, previous studies have shown that PPARα inhibits NFκB-mediated transcription in cultured cells (45, 47). We hypothesized that, compared to NFκB dimer, PPARα/NFκB heterodimer is less potent, and thus, NFκB dimer-induced transcription is inhibited when more PPARα/NFκB heterodimer is formed. To test this hypothesis, reporter gene assays were performed using the reporter harboring the m2 mutation, which allows binding of an NFκB dimer but not a PPARα/NFκB heterodimer. Although PPARα induced modest activation of the reporter harboring the intact *Il6* promoter, PPARα inhibited TNFα-induced activation of this reporter (**Fig. 6I)**. In contrast, neither PPARα-induced activation nor inhibition was observed in the reporter harboring m2. The identical result was observed when we used PA instead of PPARα. Thus,

although PPARα mediates fatty acid-induced *Il6* promoter activation, PPARα inhibits NFκB activation by other stimuli such as TNFα (**Fig. 6J**).

PPARα/NFκB heterodimer contributes to obesity-induced diastolic dysfunction

Since the PPARα/NFκB heterodimer promotes IL-6 production, it may contribute to diastolic dysfunction in response to HFD consumption. Because RXR is an authentic PPARα heterodimerization partner and strongly binds to PPARα (48), a short stretch of amino acids in RXR involved in the interaction with PPARα may competitively inhibit the binding of NFκB proteins to PPARα. RXR binds to PPARα through two independent regions, the DNA binding domain and the ligand binding domain, designated as RXRαD1 (dimerization domain 1) and RXRαD2, respectively (**Fig. 7A**). First, we tested whether full-length RXR inhibits the binding of PPARα to p50. *In vitro* binding assays revealed that full-length RXRα competitively inhibits the binding of PPARα to p50, suggesting that NFκB and RXR bind competitively to PPARα (**Fig. 7B**). We next tested whether RXRαD1 or RXRαD2 inhibits the binding of PPARα to NFκB. *In vitro* binding assays revealed that both RXRαD1 and RXRαD2 competitively inhibit the binding of PPARα to p50 (**Fig. 7C**). In contrast, as we have reported previously (49), RXRαD1 did not significantly inhibit the binding of PPARα to full-length RXRα (**Fig. S6**). These results suggest that PPARα utilizes overlapping regions to bind to NFκB and RXRα. To achieve specific inhibition of PPARα/NFκB heterodimerization, we chose RXRαD1 for two reasons. First, RXRαD1 does not inhibit the binding of PPARα to full length RXR. Second, RXRαD2 may also competitively inhibit ligand binding to endogenous RXR. To investigate whether and how RXRαD1 inhibits the DNA binding of PPARα and NFκB, DNA binding assays were performed. As shown in **Fig. 7D**, the binding of PPARα to the κB element was enhanced in the presence of p50, which was inhibited by RXRαD1. In contrast, the binding of p50 to the κB element was

partly inhibited by PPARα, which was normalized by RXRαD1. These results suggest that RXRαD1 inhibits the binding of PPARα to the κB element, which promotes p50 homodimerization on the κB element. To test whether RXRαD1 specifically inhibits fatty acid-induced *Il6* promoter activation, reporter gene assays were performed. PA-induced *Il6* promoter activation was inhibited by RXRαD1, whereas neither PA-induced PPRE activation nor TNFα-induced *Il6* promoter activation was significantly inhibited (**Fig. 7E**). Thus, RXRαD1 is an intriguing tool that specifically inhibits PPARα/NFκB heterodimerization on the κB element, but not NFκB homodimerization or PPARα/RXR heterodimerization on the PPRE. To investigate the role of the PPARα/NFκB heterodimer in mediating HFD-induced diastolic dysfunction, we generated an adeno-associated virus to induce RXRαD1 expression (AAV-*RxrαD1*). HFD-induced diastolic dysfunction was partially normalized by AAV-RXRαD1 (**Fig. 7F**). HFD-induced cytokine expression, such as Il6, was inhibited by AAV- RXRαD1, whereas authentic PPARα target genes involved in fatty acid metabolism were not significantly changed (**Fig. 7G and 7H**). The expression of RXRαD1 was verified (**Fig. 7H right panel**). To examine whether the PPARα-NFκB interaction contributes to cardiac dysfunction by promoting lipotoxicity, we measured myocardial triglyceride content in mice transduced with AAV-RXRαD1 or AAV-GFP. AAV-RXRαD1 did not significantly alter triglyceride levels in the heart (Fig. 7I). These findings suggest that PPARα-NFκB interaction does not contributes to lipotoxicity. Taken together, these results suggest that the PPARα/NFκB heterodimer mediates HFD-induced diastolic dysfunction, partly through IL-6 production.

Discussion

It is widely accepted that inflammation and pro-inflammatory cytokines drive diastolic dysfunction and cardiomyopathy in humans and mice with obesity and diabetes (50). However, the cellular sources of cytokines and the molecular mechanisms through which cytokines are

produced in the setting of obesity are poorly understood, particularly during its early stage. We here show that PPARα in *cardiomyocytes* is activated by HFD consumption in mice before histological and biochemical signs of inflammation are observed. PPARα in *cardiomyocytes* plays an essential role in mediating autocrine production of IL-6, through direct interaction with NFκB, which in turn promotes diastolic dysfunction (Fig. 7I).

Pathological role of cardiomyocytes producing IL-6

Elevated plasma levels of IL-6 are associated with an increased risk of heart failure with preserved ejection fraction (51). In addition, IL-6 infusion induces diastolic dysfunction in rats (52). Despite its importance in the pathogenesis of obesity cardiomyopathy, it has been unclear where in the body the IL-6 that drives diastolic dysfunction is produced. We showed that HFD consumption stimulates upregulation of *Il6* mRNA in cardiomyocytes. scRNA-seq further indicated that activation of immune and inflammatory signaling pathways in cardiomyocytes takes place in obesity. HFD consumption upregulated IL-6 protein in the mouse heart, an effect that was abolished in *Il6* cKO mice, suggesting that IL-6 in the cardiac tissue is produced primarily in *cardiomyocytes* during HFD consumption. Furthermore, HFD-induced diastolic dysfunction was abolished in *Il6* cKO mice. These results point to the importance of local autocrine production of IL-6 in cardiomyocytes in mediating diastolic dysfunction. Upregulation of IL-6 and diastolic dysfunction in response to HFD consumption took place before obvious histological signs of cardiac hypertrophy and fibrosis, were observed (53, 54). This also supports the mechanistic role of IL-6 as an initial driver in diastolic dysfunction.

The plasma level of IL-6 was elevated in response to HFD consumption, an effect that was abolished in (systemic) *Ppara* KO mice but not in *Ppara* cKO mice, suggesting that PPARα in non-cardiomyocytes is involved in the upregulation of IL-6 in the *plasma*. Since the plasma IL-6 level was not further increased in Tg-*Ppara* mice after HFD consumption compared to in

control mice, we speculate that PPARα-mediated production of IL-6 in cardiomyocytes does not contribute to the increased plasma IL-6 during HFD consumption. The identity of the cell type responsible for the HFD- and PPARα-dependent production of IL-6 in the plasma remains to be elucidated. Importantly, however, the suppression of diastolic dysfunction in *Ppara* cKO mice was observed even when the plasma level of IL-6 remained elevated, suggesting that IL-6 produced in *cardiomyocytes*, rather than plasma IL-6, mediates diastolic dysfunction.

The function of PPARα as a positive mediator of IL-6 production in the context of HFD consumption shown in this study is opposite to the known function of PPARα in the literature, where PPARα negatively affects inflammatory cytokine production (45). As we discuss below, we discovered that PPARα has the ability to interact with the κB element in the promoters of selected proinflammatory genes, thereby positively regulating their expression.

PPARα promotes IL-6 production in cardiomyocytes

Obesity induces pathogen-independent low grade inflammation (27). This could be a mechanism responsible for insulin resistance and diabetes (55). Despite its pathological significance, the underlying mechanism through which obesity induces inflammation is poorly understood. Protein kinase R (PKR), a serine-threonine kinase involved in protection against viral infection and endoplasmic reticular stress, plays an essential role in obesity-induced inflammation, although how PKR senses obesity remains unknown (56). Toll like receptor 4 (TLR4) may be activated by fatty acids and, in turn, activates NFκB (57). However, it remains unclear whether fatty acids act as a direct ligand for TLR4 (58). In the current study, activation of PPARα, increased IL-6 in the heart, and the development of diastolic dysfunction were all observed in the very early phase of HFD consumption, *before* the infiltration of inflammatory cells was observed in the heart. This, together with the fact that HFD-induced upregulation of IL-6 in the heart was abolished in *Ppara* cKO mice, demonstrates that myocardial upregulation of

IL-6 occurs through PPARα in cardiomyocytes, independently of infiltrating pro-inflammatory cells such as macrophages. Elimination of macrophages with clodronate failed to prevent HFD-induced diastolic dysfunction. Thus, we here propose that PPARα in *cardiomyocytes* senses increased plasma fatty acid levels, thereby stimulating transcription of proinflammatory genes.

The PPARα/NFκB heterodimer promotes *Il6* transcription through the κB element

Previous studies have shown that PPARα inhibits NFκB-induced IL-6 induction in Cos-1 cells (45). Unexpectedly, our results suggest that PPARα promotes IL-6 production during HFD consumption through an NFκB-dependent mechanism. Multiple lines of evidence support this unexpected action of PPARα. First, PPARα is able to stimulate the *Il6* promoter, which requires the presence of the PPARα activation domain and is stimulated in the presence of PPARα ligands. PPARα's ability to stimulate the *Il6* reporter promoter does not require the PPRE-like element (DR3) but critically depends on the presence of both NFκB and the κB element. Second, PPARα and p50/RelA directly interact with one another in the nucleus. Third, PPARα has the ability to interact with the κB element in the *Il6* promoter both *in vitro* and *in vivo*. DNA binding assays suggest that the ability of PPARα to interact with the κB element in the *Il6* promoter strictly depends upon the sequence of the κB element and is enhanced in the presence of either p50 or RelA. Thus, PPARα binding to the κB element in the *Il6* promoter is promoted in the presence of a binding partner, namely p50 or RelA. Fourth, the presence of a minigene encoding RXRαD1, a decoy that interferes with the PPARα/NFκB interaction, prevents upregulation of *Il6* in response to HFD consumption. Finally, unbiased ChIP-sequencing analyses showed that PPARα and RelA/p50 have overlapping peaks near the κB site in the *Il6* promoter. The level of PPARα binding to the κB element in the *Il6* and *Tnfa* promoters was as high as to the authentic PPRE in the *Acox1* and *Cpt1b* promoters. These

results support the idea that the PPARα/NFκB heterodimer can stimulate transcription of *Il6* through stimulation of the κB element. It should be noted that PPARα binding to the κB element is sequence-specific and only a subset of κB elements, such as those in the *Il6* and *Tnfa* promoters, possess a PPARα preferred binding sequence. Whether PPARα binds to the κB elements in the promoters of other genes needs to be tested in an unbiased manner.

How does PPARα have directionally opposite effects on NFκB-mediated transcription in cardiomyocytes and other cell types? We found that the PPARα/NFκB heterodimer induces transcriptional activation less potently than the authentic NFκB dimer. ChIP sequencing analyses showed that both endogenous PPARα and NFκB bind to the κB element at baseline and during HFD consumption. However, NFκB predominantly binds to the κB element in response to canonical stimuli. Under these conditions, overexpression of PPARα inhibits κB-mediated transcription, most likely by replacing the authentic NFκB homodimer with the PPARα/NFκB heterodimer, which activates transcription less potently than the NFκB homodimer. Thus, PPARα stimulates the κB element bound by the PPARα/NFκB heterodimer in a PPARα ligand-dependent manner, whereas upregulation of PPARα may negatively affect stimulation of the κB element by the authentic NFκB dimer. The timing and the mechanism that determines whether the κB element is controlled by the PPARα/NFκB heterodimer or the NFκB homodimer remain to be elucidated.

Physiological role of PPARα-NFκB-induced low grade inflammatory reaction

Several physiological roles of obesity-induced low grade inflammation have been proposed. Obesity induces tissues damages due to metabolic and cellular stress. Low-grade inflammatory signaling may initially function as an adaptive response that promotes tissue repair and remodeling (59). A better understanding of the physiological significance of this pathway will be critical for its therapeutic exploitation, as it may enable the identification of patient populations in

whom such interventions would be beneficial or detrimental, allow anticipation of potential side effects, and facilitate the development of strategies that selectively suppress pathological signaling while preserving beneficial functions.

Study limitations

Although the short-term HFD model enabled us to dissect the early molecular mechanism, it may not fully recapitulate cardiac remodeling observed during the chronic phase of obesity cardiomyopathy. In addition, PPARα possesses multiple functions in the heart, including transcription of genes involved in fatty acid oxidation. Thus, the significance of PPARα-NFκB-mediated upregulation of inflammatory cytokines and other functions of PPARα during longer term obesity cardiomyopathy needs to be elucidated with time-dependent conditional downregulation of the PPARα-NFκB pathway.

The molecular mechanism through which IL-6 mediates diastolic dysfunction remains to be elucidated. IL-6 downregulates Atp2a2 in cultured ventricular myocytes (60). Given that Atp2a2 mediates calcium reuptake into the sarcoplasmic reticulum thereby facilitating cardiomyocyte relaxation, a decrease in Atp2a2 may contribute to impaired diastolic function. In addition, HFD consumption activates Stat3, a major downstream effector of IL-6, in a PPARα-dependent manner. JAK/Stat3 regulates cellular mechanisms relevant to cardiac fibrosis and increased stiffness (40). Although PSR staining showed no overt cardiac fibrosis at the early phase (1 month of HFD), this does not exclude the presence of subtle extracellular matrix remodeling may still occur below its detection limit. Even low-levels of fibrosis undetectable by standard histologyl can increase myocardial stiffness and cause diastolic dysfunction (61). Thus, it is possible that IL-6 mediates diastolic dysfunction through regulation of cardiac fibrosis as well as myocardial stiffness.

Sex differences in diastolic dysfunction

In humans, women exhibit better insulin sensitivity, lower visceral fat, and reduced circulating free fatty acids (62). However, the prevalence of HFpEF is consistently higher in women than in men (63). Our study shows that PPARα functions dichotomously during HFD consumption: while PPARα supports metabolic resilience, it can also promote IL-6 expression. Whether sex-specific modification of PPARα exists and, if so, how it affects the PPARα-NFκB pathway during obesity remain to be clarified.

Therapeutic interventions for diastolic dysfunction

Based on the molecular mechanism mediating the autocrine production of IL-6 in cardiomyocytes during HFD consumption, inhibiting PPARα in a cardiomyocyte-specific manner may prevent the development of diastolic dysfunction during the early phase of obesity. Since transcription of *Il6* in obesity is most likely initiated through fatty acid ligand binding to the preexisting PPARα-NFκB complex on the *Il6* promoter, reducing the plasma level of fatty acids, by reducing obesity through lifestyle adjustments, should prevent upregulation of IL-6. Alternatively, more direct interventions targeting PPARα may be considered. It is important to note, however, that, since PPARα plays an essential role in fatty acid metabolism, a major source of energy in the heart, inhibiting every function of PPARα may cause undesirable side effects long term. Consistent with this notion, several *Ppara* cKO mice exhibited systolic dysfunction at baseline, which was normalized upon HFD feeding (Fig. 2B). We speculate that this reflects the critical role of fatty acid metabolism in maintaining basal cardiac energetics. Loss of PPARα may impair myocardial fatty acid utilization, resulting in systolic dysfunction in some animals, whereas increased fatty acid supply during HFD feeding may partially compensate for this defect and normalize cardiac function. Thus, specific interference with PPARα/NFκB heterodimerization using the minigene derived from *Rxra* (*RxraD1*) could

represent a better strategy for preventing early activation of the proinflammatory mechanism without affecting other potentially important functions of PPAR. Although we confirmed that the minigene does not interfere with the interaction between PPARα and RXRα, further investigation is required to evaluate the selectivity of the minigene against other interacting partners of PPARα. More accurate mapping of the PPARα-p50/RelA interacting domain will be essential for the rational design of highly specific small-molecule antagonists that selectively disrupt this interaction. In addition, delivering the molecule inhibiting the PPARα/NFκB interaction *in a cardiomyocyte-specific manner*, using nanoparticle approaches, should also prevent undesirable side effects.

In summary, we show that PPARα-NFκB-mediated autocrine production of IL-6 plays an important role in mediating diastolic dysfunction during the early phase of obesity cardiomyopathy. A better understanding of the dichotomous functions of PPARα and specific molecular mechanisms mediating their effects should lead to specific and effective treatment to prevents the development of cardiomyopathy in obesity patients.

METHODS

For other experimental procedures, see Supplemental Methods.

Sex as a biological variant

We used mice of both sexes in all experiments. Cultured cardiomyocytes were prepared from mice and rats of both sexes.

Statistical methods and error bars

Normality was tested with the Shapiro-Wilk normality test. If the data exhibited a normal distribution, pairwise testing was performed with the Student's *t* test and multiple group comparisons were performed by 1-way ANOVA, followed by Tukey post-test. If the data failed normality testing, pairwise testing was performed with the non-parametric Mann-Whitney *U* test and multiple group comparisons were performed by the non-parametric Kruskal-Wallis test, followed by Dunn's post-test. $P<0.05$ was defined as statistically significant and indicated by a filled asterisk. All error bars represent S. E. M.

Study Approval

All animal procedures were reviewed and approved by the Institutional Animal Care and Use Committee (IACUC) of Rutgers Biomedical and Health Sciences, Newark, New Jersey, USA.

Data availability

Single-cell RNA-seq data are deposited in NCBI GEO under accession code GE317479. ChIP-seq data are deposited in NCBI GEO under accession code GE316422. Supporting data values are provided in oka.sdva.

Acknowledgements:

The authors thank Daniela Zablocki for critical reading of the manuscript.

Author Contributions

S.O. designed the study, performed most of the experiments, analyzed data, and interpreted results. K.S. maintained animal lines fed HFD. S.B. performed histological analyses. K.S., A.C. Y.M. and S.K. performed Western blot analyses. E.S. obtained and analyzed the scRNA-seq data. P.Z. performed PV loop analyses. A.S. and Y.N. performed echocardiographic measurements and analyses. J.B. purified recombinant proteins. J.F. and D.D. performed FACS analyses. S.O. and J.S. conceived the ideas and wrote the manuscript. J.S. oversaw the entire study and maintains experimental resources and environment. All authors reviewed and approved the manuscript for publication.

Sources of Funding:

This work was supported in part by the New Jersey Health Foundation (PC-56-16), American Heart Association (AHA) Transformational Project Award 19TPA34850170 (S.O.), U.S. Public Health Service Grants HL91469, HL102738, HL112330, HL138720, HL144626, and HL150881, AHA Merit Award 20 Merit 35120374 (J.S.), and by the Fondation Leducq Transatlantic Network of Excellence 15CVD04 (J.S.).

Disclosures:

None.

References

1. Collaborators GBDO, Afshin A, Forouzanfar MH, Reitsma MB, Sur P, Estep K, et al. Health Effects of Overweight and Obesity in 195 Countries over 25 Years. *N Engl J Med.* 2017;377(1):13–27.

2. Jia G, Hill MA, and Sowers JR. Diabetic Cardiomyopathy: An Update of Mechanisms Contributing to This Clinical Entity. *Circ Res.* 2018;122(4):624–38.

3. Seferovic PM, and Paulus WJ. Clinical diabetic cardiomyopathy: a two-faced disease with restrictive and dilated phenotypes. *European heart journal.* 2015;36(27):1718–27, 27a–27c.

4. Greene SJ, and Butler J. Primary Prevention of Heart Failure in Patients With Type 2 Diabetes Mellitus. *Circulation.* 2019;139(2):152–4.

5. Berg AH, and Scherer PE. Adipose tissue, inflammation, and cardiovascular disease. *Circ Res.* 2005;96(9):939–49.

6. Wilck N, Marko L, Balogh A, Kraker K, Herse F, Bartolomaeus H, et al. Nitric oxide-sensitive guanylyl cyclase stimulation improves experimental heart failure with preserved ejection fraction. *JCI Insight.* 2018;3(4).

7. Prabhu SD. Cytokine-induced modulation of cardiac function. *Circ Res.* 2004;95(12):1140–53.

8. Daryabor G, Kabelitz D, and Kalantar K. An update on immune dysregulation in obesity-related insulin resistance. *Scand J Immunol.* 2018:e12747.

9. Spranger J, Kroke A, Mohlig M, Hoffmann K, Bergmann MM, Ristow M, et al. Inflammatory cytokines and the risk to develop type 2 diabetes: results of the prospective population-based European Prospective Investigation into Cancer and Nutrition (EPIC)-Potsdam Study. *Diabetes.* 2003;52(3):812–7.

10. Qu D, Liu J, Lau CW, and Huang Y. IL-6 in diabetes and cardiovascular complications. *Br J Pharmacol.* 2014;171(15):3595–603.

11. Ko HJ, Zhang Z, Jung DY, Jun JY, Ma Z, Jones KE, et al. Nutrient stress activates inflammation and reduces glucose metabolism by suppressing AMP-activated protein kinase in the heart. *Diabetes.* 2009;58(11):2536–46.

12. Savvatis K, Muller I, Frohlich M, Pappritz K, Zietsch C, Hamdani N, et al. Interleukin-6 receptor inhibition modulates the immune reaction and restores titin phosphorylation in experimental myocarditis. *Basic Res Cardiol.* 2014;109(6):449.

13. Boden G, She P, Mozzoli M, Cheung P, Gumireddy K, Reddy P, et al. Free fatty acids produce insulin resistance and activate the proinflammatory nuclear factor-kappaB pathway in rat liver. *Diabetes.* 2005;54(12):3458–65.

14. Oka S, Alcendor R, Zhai P, Park JY, Shao D, Cho J, et al. PPARalpha-Sirt1 complex mediates cardiac hypertrophy and failure through suppression of the ERR transcriptional pathway. *Cell Metab.* 2011;14(5):598–611.

15. Oka S, Zhai P, Yamamoto T, Ikeda Y, Byun J, Hsu CP, et al. Peroxisome Proliferator Activated Receptor-alpha Association With Silent Information Regulator 1 Suppresses Cardiac Fatty Acid Metabolism in the Failing Heart. *Circulation Heart failure.* 2015;8(6):1123–32.

16. Tzeng J, Byun J, Park JY, Yamamoto T, Schesing K, Tian B, et al. An Ideal PPAR Response Element Bound to and Activated by PPARalpha. *PLoS One.* 2015;10(8):e0134996.

17. Warren JS, Oka SI, Zablocki D, and Sadoshima J. Metabolic reprogramming via PPARalpha signaling in cardiac hypertrophy and failure: From metabolomics to epigenetics. *Am J Physiol Heart Circ Physiol.* 2017;313(3):H584–H96.

18. Drosatos K, Pollak NM, Pol CJ, Ntziachristos P, Willecke F, Valenti MC, et al. Cardiac Myocyte KLF5 Regulates Ppara Expression and Cardiac Function. *Circ Res.* 2016;118(2):241–53.

19. Nakamura M, and Sadoshima J. Cardiomyopathy in obesity, insulin resistance or diabetes. *J Physiol.* 2019.

20. Finck BN, Han X, Courtois M, Aimond F, Nerbonne JM, Kovacs A, et al. A critical role for PPARalpha-mediated lipotoxicity in the pathogenesis of diabetic cardiomyopathy: modulation by dietary fat content. *Proc Natl Acad Sci U S A.* 2003;100(3):1226–31.

21. Guerre-Millo M, Rouault C, Poulain P, Andre J, Poitout V, Peters JM, et al. PPAR-alpha-null mice are protected from high-fat diet-induced insulin resistance. *Diabetes.* 2001;50(12):2809–14.

22. Wu R, Chang HC, Khechaduri A, Chawla K, Tran M, Chai X, et al. Cardiac-specific ablation of ARNT leads to lipotoxicity and cardiomyopathy. *J Clin Invest.* 2014;124(11):4795–806.

23. Alvarez-Guardia D, Palomer X, Coll T, Serrano L, Rodriguez-Calvo R, Davidson MM, et al. PPARbeta/delta activation blocks lipid-induced inflammatory pathways in mouse heart and human cardiac cells. *Biochim Biophys Acta.* 2011;1811(2):59–67.

24. Mulvey CK, Ferguson JF, Tabita-Martinez J, Kong S, Shah RY, Patel PN, et al. Peroxisome Proliferator-Activated Receptor-alpha Agonism With Fenofibrate Does Not Suppress Inflammatory Responses to Evoked Endotoxemia. *J Am Heart Assoc.* 2012;1(4):e002923.

25. Qi Y, Jiang C, Tanaka N, Krausz KW, Brocker CN, Fang ZZ, et al. PPARalpha-dependent exacerbation of experimental colitis by the hypolipidemic drug fenofibrate. *Am J Physiol Gastrointest Liver Physiol.* 2014;307(5):G564–73.

26. Zhang JZ, and Ward KW. WY-14 643, a selective PPAR{alpha} agonist, induces proinflammatory and proangiogenic responses in human ocular cells. *Int J Toxicol.* 2010;29(5):496–504.

27. Gregor MF, and Hotamisligil GS. Inflammatory mechanisms in obesity. *Annual review of immunology.* 2011;29:415–45.

28. Wang CY, and Liao JK. A mouse model of diet-induced obesity and insulin resistance. *Methods Mol Biol.* 2012;821:421–33.

29. Borlaug BA, and Paulus WJ. Heart failure with preserved ejection fraction: pathophysiology, diagnosis, and treatment. *European heart journal.* 2011;32(6):670–9.

30. Coppi F, Pagnoni G, Grossule F, Nassar A, Maini A, Masaracchia G, et al. Gender-Specific Differences in Diastolic Dysfunction and HFpEF: Pathophysiology, Diagnosis, and Therapeutic Strategies. *J Cardiovasc Dev Dis.* 2025;12(6).

31. Roh J, Hill JA, Singh A, Valero-Munoz M, and Sam F. Heart Failure With Preserved Ejection Fraction: Heterogeneous Syndrome, Diverse Preclinical Models. *Circ Res.* 2022;130(12):1906–25.

32. Martos R, Baugh J, Ledwidge M, O'Loughlin C, Conlon C, Patle A, et al. Diastolic heart failure: evidence of increased myocardial collagen turnover linked to diastolic dysfunction. *Circulation.* 2007;115(7):888–95.

33. Duncan JG, Bharadwaj KG, Fong JL, Mitra R, Sambandam N, Courtois MR, et al. Rescue of cardiomyopathy in peroxisome proliferator-activated receptor-alpha transgenic mice by deletion of lipoprotein lipase identifies sources of cardiac lipids and peroxisome proliferator-activated receptor-alpha activators. *Circulation.* 2010;121(3):426–35.

34. Finck BN, Lehman JJ, Leone TC, Welch MJ, Bennett MJ, Kovacs A, et al. The cardiac phenotype induced by PPARalpha overexpression mimics that caused by diabetes mellitus. *J Clin Invest.* 2002;109(1):121–30.

35. Glezeva N, and Baugh JA. Role of inflammation in the pathogenesis of heart failure with preserved ejection fraction and its potential as a therapeutic target. *Heart failure reviews.* 2014;19(5):681–94.

36. Gwechenberger M, Mendoza LH, Youker KA, Frangogiannis NG, Smith CW, Michael LH, et al. Cardiac myocytes produce interleukin-6 in culture and in viable border zone of reperfused infarctions. *Circulation.* 1999;99(4):546–51.

37. Baker RG, Hayden MS, and Ghosh S. NF-kappaB, inflammation, and metabolic disease. *Cell metabolism.* 2011;13(1):11–22.

38. Nguyen T, Du J, and Li YC. A protocol for macrophage depletion and reconstitution in a mouse model of sepsis. *STAR Protoc.* 2021;2(4):101004.

39. Lin X, Korai A, Nakazawa Y, Tago K, and Funakoshi-Tago M. The critical role of the phosphorylation of STAT3 at Y705 in ALCL-associated NPM-ALK-induced transforming activity. *Cell Signal.* 2025:112128.

40. Harhous Z, Booz GW, Ovize M, Bidaux G, and Kurdi M. An Update on the Multifaceted Roles of STAT3 in the Heart. *Front Cardiovasc Med.* 2019;6:150.

41. Chew GS, Myers S, Shu-Chien AC, and Muhammad TS. Interleukin-6 inhibition of peroxisome proliferator-activated receptor alpha expression is mediated by JAK2- and PI3K-induced STAT1/3 in HepG2 hepatocyte cells. *Mol Cell Biochem.* 2014;388(1-2):25–37.

42. Marr LT, Ocampo J, Clark DJ, and Hayes JJ. Global histone protein surface accessibility in yeast indicates a uniformly loosely packed genome with canonical nucleosomes. *Epigenetics Chromatin.* 2021;14(1):5.

43. Vega RB, Huss JM, and Kelly DP. The coactivator PGC-1 cooperates with peroxisome proliferator-activated receptor alpha in transcriptional control of nuclear genes encoding mitochondrial fatty acid oxidation enzymes. *Mol Cell Biol.* 2000;20(5):1868–76.

44. Kunsch C, Ruben SM, and Rosen CA. Selection of optimal kappa B/Rel DNA-binding motifs: interaction of both subunits of NF-kappa B with DNA is required for transcriptional activation. *Mol Cell Biol.* 1992;12(10):4412–21.

45. Delerive P, De Bosscher K, Besnard S, Vanden Berghe W, Peters JM, Gonzalez FJ, et al. Peroxisome proliferator-activated receptor alpha negatively regulates the vascular inflammatory gene response by negative cross-talk with transcription factors NF-kappaB and AP-1. *J Biol Chem.* 1999;274(45):32048–54.

46. Dowell P, Ishmael JE, Avram D, Peterson VJ, Nevrivy DJ, and Leid M. Identification of nuclear receptor corepressor as a peroxisome proliferator-activated receptor alpha interacting protein. *J Biol Chem.* 1999;274(22):15901–7.

47. Delerive P, Gervois P, Fruchart JC, and Staels B. Induction of IkappaBalpha expression as a mechanism contributing to the anti-inflammatory activities of peroxisome proliferator-activated receptor-alpha activators. *The Journal of biological chemistry.* 2000;275(47):36703–7.

48. Schoonjans K, Staels B, and Auwerx J. Role of the peroxisome proliferator-activated receptor (PPAR) in mediating the effects of fibrates and fatty acids on gene expression. *J Lipid Res.* 1996;37(5):907–25.

49. Oka SI, Zhai P, Yamamoto T, Ikeda Y, Byun J, Hsu CP, et al. PPARalpha Association With Sirt1 Suppresses Cardiac Fatty Acid Metabolism in the Failing Heart. *Circulation Heart failure.* 2015.

50. Paulus WJ, and Zile MR. From Systemic Inflammation to Myocardial Fibrosis: The Heart Failure With Preserved Ejection Fraction Paradigm Revisited. *Circulation research.* 2021;128(10):1451–67.

51. Chia YC, Kieneker LM, van Hassel G, Binnenmars SH, Nolte IM, van Zanden JJ, et al. Interleukin 6 and Development of Heart Failure With Preserved Ejection Fraction in the General Population. *J Am Heart Assoc.* 2021;10(11):e018549.

52. Melendez GC, McLarty JL, Levick SP, Du Y, Janicki JS, and Brower GL. Interleukin 6 mediates myocardial fibrosis, concentric hypertrophy, and diastolic dysfunction in rats. *Hypertension.* 2010;56(2):225–31.

53. Nakamura M, Liu T, Husain S, Zhai P, Warren JS, Hsu CP, et al. Glycogen Synthase Kinase-3alpha Promotes Fatty Acid Uptake and Lipotoxic Cardiomyopathy. *Cell Metab.* 2019;29(5):1119–34 e12.

54. Oka SI, Byun J, Huang CY, Imai N, Ralda G, Zhai P, et al. Nampt Potentiates Antioxidant Defense in Diabetic Cardiomyopathy. *Circ Res.* 2021;129(1):114–30.

55. Hotamisligil GS. Inflammation, metaflammation and immunometabolic disorders. *Nature.* 2017;542(7640):177–85.

56. Nakamura T, Furuhashi M, Li P, Cao H, Tuncman G, Sonenberg N, et al. Double-stranded RNA-dependent protein kinase links pathogen sensing with stress and metabolic homeostasis. *Cell.* 2010;140(3):338–48.

57. Shi H, Kokoeva MV, Inouye K, Tzameli I, Yin H, and Flier JS. TLR4 links innate immunity and fatty acid-induced insulin resistance. *J Clin Invest.* 2006;116(11):3015–25.

58. Lancaster GI, Langley KG, Berglund NA, Kammoun HL, Reibe S, Estevez E, et al. Evidence that TLR4 Is Not a Receptor for Saturated Fatty Acids but Mediates Lipid-Induced Inflammation by Reprogramming Macrophage Metabolism. *Cell Metab.* 2018;27(5):1096–110 e5.

59. Oliveira MC, Marcelin G, Gautier EL, and Ferreira AVM. Editorial: Inflammation in Obesity: From Physiological to Pathological Aspects. *Front Nutr.* 2022;9:870131.

60. Villegas S, Villarreal FJ, and Dillmann WH. Leukemia Inhibitory Factor and Interleukin-6 downregulate sarcoplasmic reticulum Ca2+ ATPase (SERCA2) in cardiac myocytes. *Basic Res Cardiol.* 2000;95(1):47–54.

61. Travers JG, Wennersten SA, Pena B, Bagchi RA, Smith HE, Hirsch RA, et al. HDAC Inhibition Reverses Preexisting Diastolic Dysfunction and Blocks Covert Extracellular Matrix Remodeling. *Circulation.* 2021;143(19):1874–90.

62. Geer EB, and Shen W. Gender differences in insulin resistance, body composition, and energy balance. *Gend Med.* 2009;6 Suppl 1(Suppl 1):60–75.

63. Sotomi Y, Hikoso S, Nakatani D, Mizuno H, Okada K, Dohi T, et al. Sex Differences in Heart Failure With Preserved Ejection Fraction. *J Am Heart Assoc.* 2021;10(5):e018574.

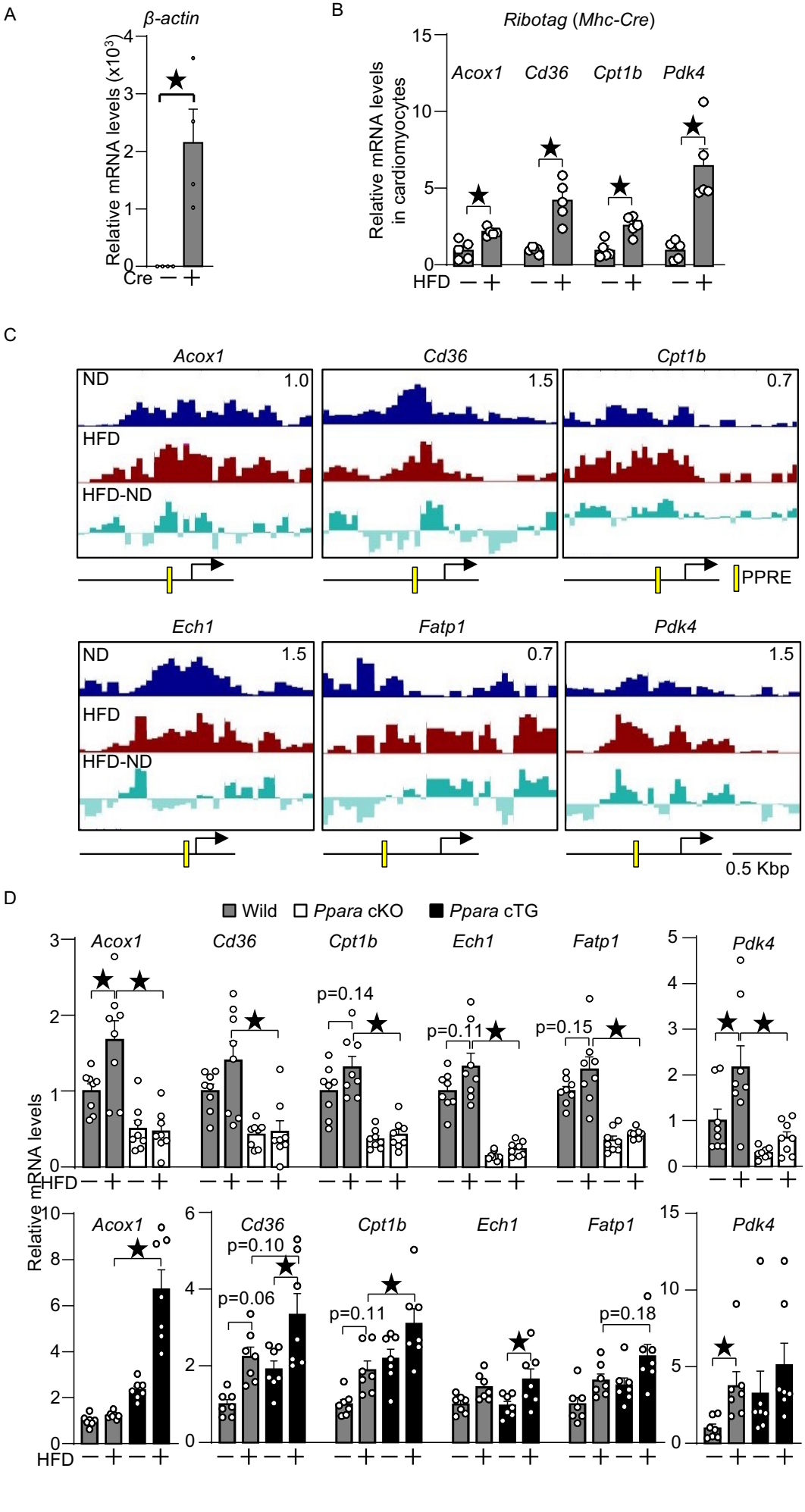
A
β-actin
Relative mRNA levels (x10³)
Cre
B
Ribotag (Mhc-Cre)
Relative mRNA levels in cardiomyocytes
Acox1
Cd36
Cpt1b
Pdk4
HFD
C
Acox1
Cd36
Cpt1b
ND
HFD
HFD-ND
PPRE
Ech1
Fatp1
Pdk4
0.5 Kbp
D
Wild
Ppara cKO
Ppara cTG
Relative mRNA levels
HFD
p=0.14
p=0.11
p=0.15
p=0.10
p=0.06
p=0.11
p=0.18

Figure 1. PPARα is functional under high-fat diet (HFD) consumption conditions. (A) Successful mRNA isolation from cardiomyocyte-specific *Ribo-Tag* mice. (B) HFD induces PPAR target gene expression in cardiomyocytes in the heart *in vivo*. (A-B) Ribosome-associated RNA was isolated with HA-Rpl22, which is expressed in cardiomyocytes in a *Myh6*-Cre-dependent manner. Expression of indicated genes was examined. (C) PPARα localizes to near PPRE in the promoters of its target genes, with heterogeneous binding responses to HFD consumption. ChIP-seq was performed once using pooled heart samples from three mice after one month of HFD feeding. The Y-axis in the UCSC genome browser is indicated at top right (0.7 - 1.5). Difference in PPARα occupancy between ND and HFD conditions is shown as HFD–ND. (D) HFD-induced PPARα target gene expression is inhibited in *Ppara* cKO but enhanced in Tg-*Ppara* mice. Expression levels of indicated PPAR target genes after 1 month of HFD consumption were examined in *Ppara* KO and Tg-*Ppara* mice. The numbers of mice examined in each experimental group were: 4 (A), 5 (B) and 7-8 (C). Statistical significance is indicated by a star and was assessed using Student's t-test in (A) and (B), the Kruskal–Wallis test for PDK4 in (C), and ANOVA for other comparisons in (C).

Figure 2

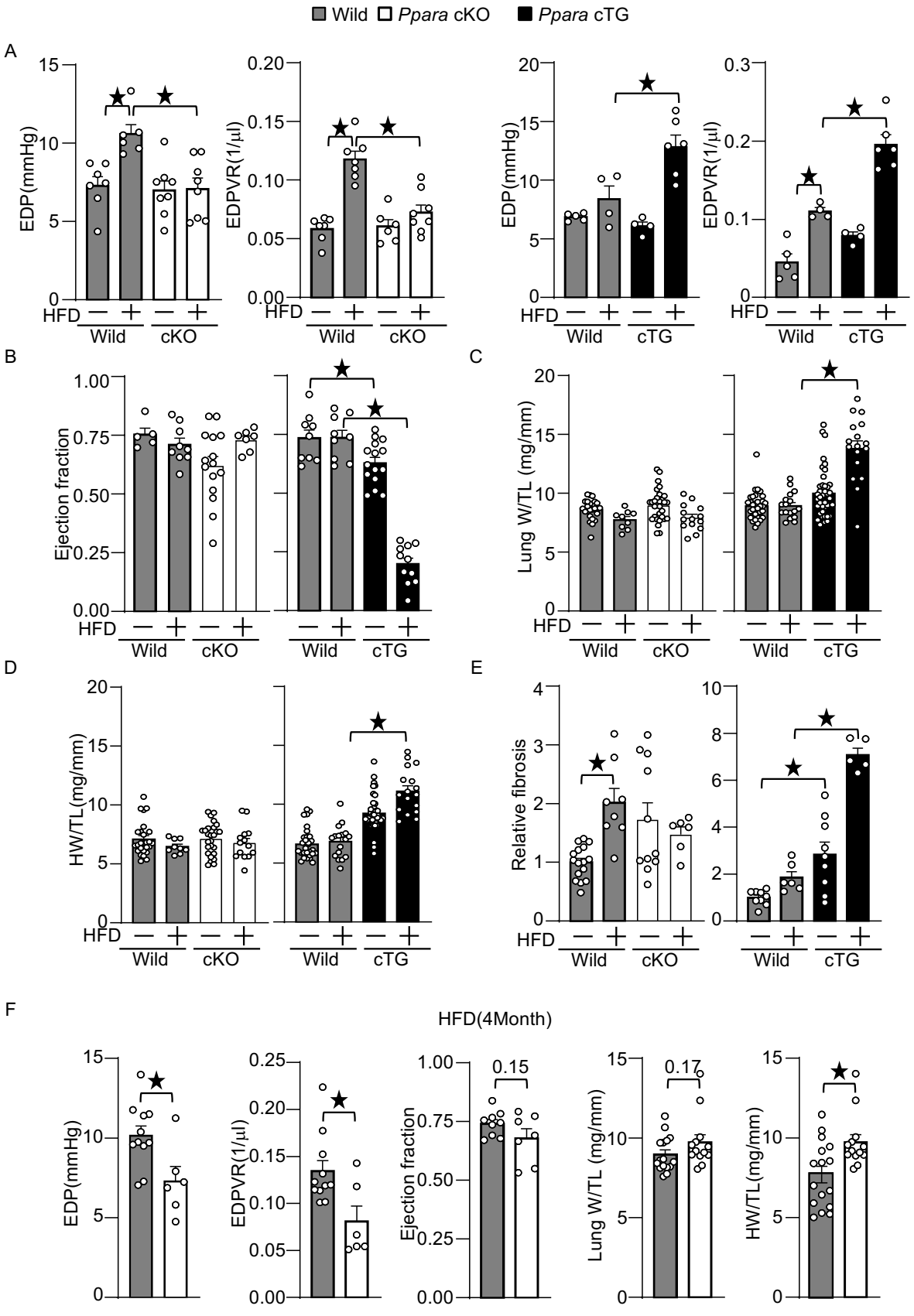
Wild
Ppara cKO
Ppara cTG
A
EDP(mmHg)
EDPVR(1/μl)
HFD
Wild
cKO
cTG
B
Ejection fraction
C
Lung W/TL (mg/mm)
D
HW/TL(mg/mm)
E
Relative fibrosis
F
HFD(4Month)
0.15
0.17

Figure 2. PPARα mediates HFD-induced diastolic dysfunction. (A) HFD-induced diastolic dysfunction is ameliorated in *Ppara c*KO but exacerbated in Tg-*Ppara* mice. HFD: 1 month. (B) After 1 month of HFD feeding, cardiac systolic function was unchanged in *Ppara* KO and *Ppara* cKO, but impaired in Tg-*Ppara* mice. (C) Lung weight/Tibia length ratio. (D) Heart weight/Tibia length ratio. (E) HFD-induced increases in body weight were not significantly changed in *Ppara* KO, *Ppara* cKO or Tg-*PPARα* mice. HFD: 1 month. (E) HFD-induced cardiac fibrosis was ameliorated in *Ppara* KO but exacerbated in Tg-*Ppara* mice. HFD: 3 months (*Ppara* KO and *Ppara* cKO) and 1 month (Tg-*Ppara*). (F) The role of cardiomyocyte PPARα in cardiac pathology during prolonged HFD feeding. *Ppara* cKO mice were fed HFD for 4 months. Diastolic function (EDP, EDPVR), systolic function (ejection fraction), pulmonary congestion (lung weight/TL), and cardiac hypertrophy (HW/TL) were assessed to evaluate the progression of cardiac pathology. The numbers of mice examined in each experimental group were: 4-7 (A), 5-15 (B), 9-41 (C), 9-40 (D), 5-16 (E), 6-11 (F, EDP and EDPVR), 7-9 (F, ejection fraction), and 13-16 (F, Lung W/TL and HW/TL). Statistical significance is indicated by a star and was assessed using the Kruskal–Wallis test for Tg-*Ppara* in (C), Tg-*Ppara* in (D), and *Ppara* cKO in (E), the Student's t-test in (F, EDP, ejection fraction), the Mann–Whitney U test in (F, EDPVR, Lung W/TL and HW/TL), and ANOVA for other comparisons in (A-E).

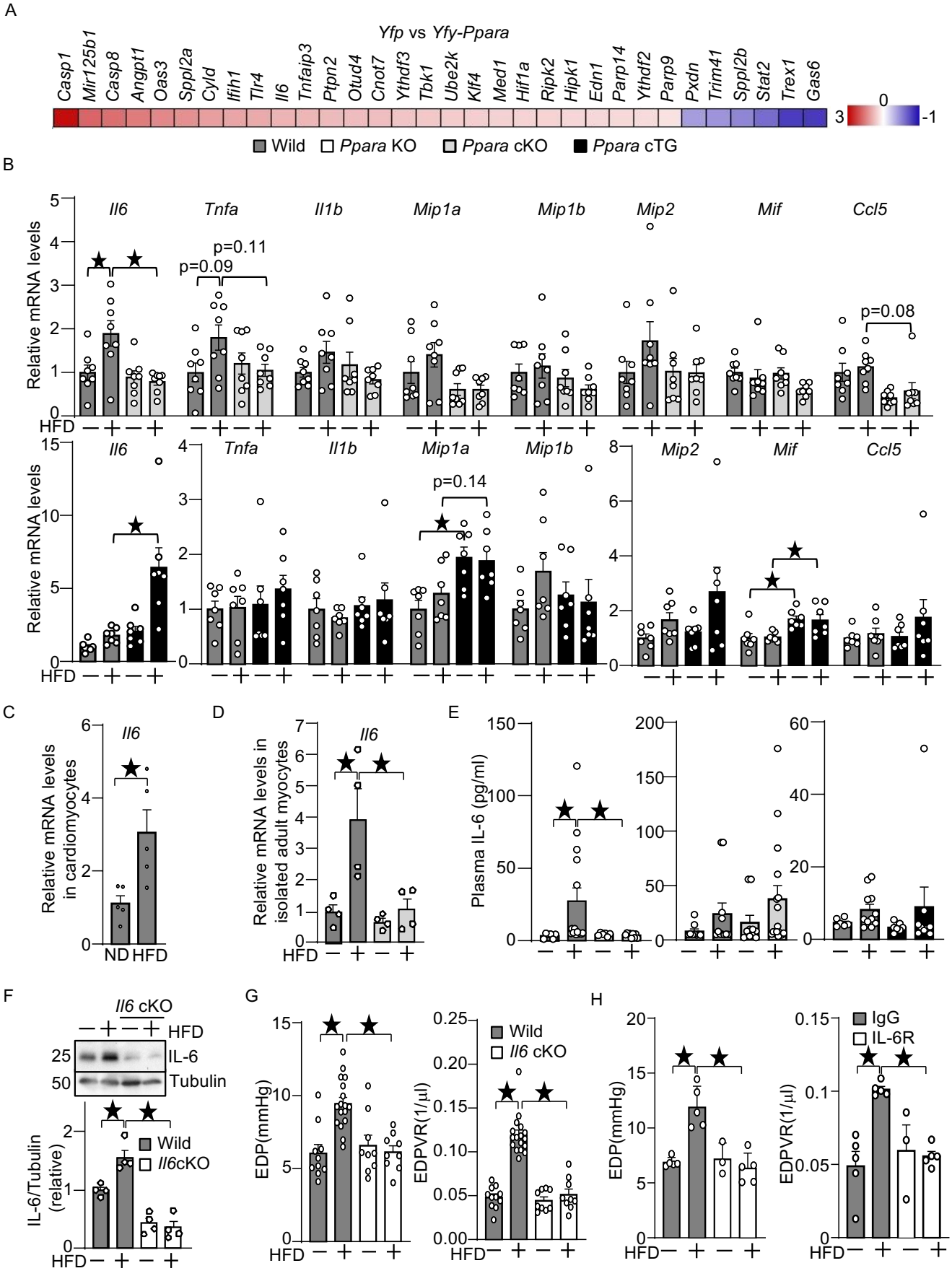
A
Yfp vs Yfy-Ppara
Casp1
Mir125b1
Casp8
Angpt1
Oas3
Sppl2a
Cyld
Ifih1
Tlr4
Il6
Tnfaip3
Ptpn2
Otud4
Cnot7
Ythdf3
Tbk1
Ube2k
Klf4
Med1
Hif1a
Ripk2
Hipk1
Edn1
Parp14
Ythdf2
Parp9
Pxdn
Trim41
Sppl2b
Stat2
Trex1
Gas6
3
0
-1
Wild
Ppara KO
Ppara cKO
Ppara cTG
B
Relative mRNA levels
Il6
Tnfa
Il1b
Mip1a
Mip1b
Mip2
Mif
Ccl5
p=0.11
p=0.09
p=0.08
p=0.14
HFD
C
Relative mRNA levels in cardiomyocytes
ND HFD
D
Relative mRNA levels in isolated adult myocytes
E
Plasma IL-6 (pg/ml)
F
Il6 cKO
HFD
IL-6
Tubulin
25
50
IL-6/Tubulin (relative)
Wild
Il6cKO
G
EDP(mmHg)
EDPVR(1/μl)
Wild
Il6 cKO
H
IgG
IL-6R

Figure 3. PPARα mediates HFD-induced inflammatory cytokine expression, thereby promoting diastolic dysfunction. (A) PPARα upregulates cytokine and inflammation related genes. RNA-seq was performed in H9c2 cells with *Yfp-Ppara* overexpression. Among the genes listed in "GOBP Regulation of Response to Cytokine Stimulus", those whose expression was significantly changed by PPARα overexpression are shown in a heatmap. (B) Expression levels of indicated cytokines after 1 month of HFD consumption in *Ppara* KO, *Ppara* cKO and Tg-*Ppara* mice. N=6-8. (C) Cardiomyocytes express *Il6*. After 1 month of HFD consumption, *Il6* expression was examined with *Ribo-tag* mice. (D) PPARα-dependent *Il6* induction in adult cardiomyocytes. The mRNA level of *Il6* was examined in adult cardiomyocytes isolated from *Ppara* cKO mice fed HFD for 1 month. (E) Plasma levels of IL-6 in *Ppara* KO, *Ppara* cKO and Tg-*Ppara* mice. (F) IL-6 induction in response to HFD is inhibited in *Il6* cKO mice. Protein levels of IL-6 were examined in heart lysates of *Il6*cKO mice after 1 month of HFD consumption. (G) HFD-induced diastolic dysfunction is ameliorated in *Il6* cKO mice. (H) HFD-induced diastolic dysfunction is ameliorated with anti-IL-6R antibody. The numbers of mice examined in each experimental group were: 7-8 (B), 5 (C), 4 (D), 6-16 (E), 4(F), 9-17 (G) and 3-5 (H). Statistical significance is indicated by a star and was assessed using the Kruskal–Wallis test for Tg-*Ppara* in (C), Tg-*Ppara* in (D), and *Ppara* cKO in (E), and ANOVA for other comparisons in (A-E).

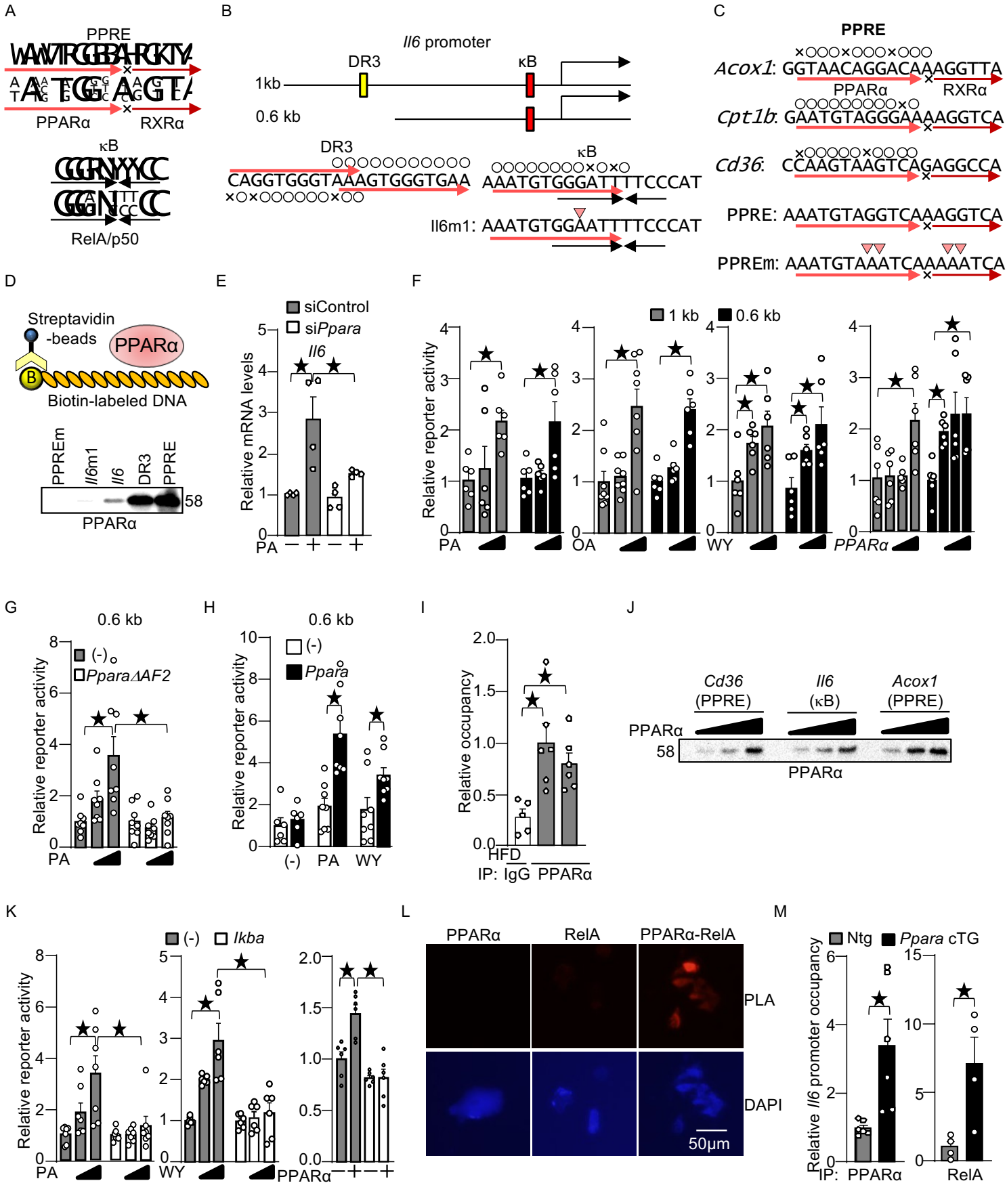
A
PPRE
PPARα
RXRα
κB
RelA/p50
B
Il6 promoter
DR3
κB
1kb
0.6 kb
CAGGTGGGTAAAGTGGGTGAA
AAATGTGGGATTTTCCCAT
Il6m1: AAATGTGGAATTTTCCCAT
C
PPRE
Acox1: GGTAACAGGACAAAGGTTA
Cpt1b: GAATGTAGGGAAAAGGTCA
Cd36: CCAAGTAAGTCAGAGGCCA
PPRE: AAATGTAGGTCAAAGGTCA
PPREm: AAATGTAAATCAAAAATCA
D
Streptavidin
-beads
PPARα
Biotin-labeled DNA
PPREm
Il6m1
Il6
DR3
PPRE
58
PPARα
E
siControl
siPpara
Il6
Relative mRNA levels
PA
F
1 kb
0.6 kb
Relative reporter activity
PA
OA
WY
PPARα
G
0.6 kb
(-)
PparaΔAF2
Relative reporter activity
PA
H
0.6 kb
(-)
Ppara
Relative reporter activity
(-)
PA
WY
I
Relative occupancy
HFD
IP: IgG
PPARα
J
Cd36
(PPRE)
Il6
(κB)
Acox1
(PPRE)
PPARα
58
PPARα
K
(-)
Ikba
Relative reporter activity
PA
WY
PPARα
L
PPARα
RelA
PPARα-RelA
PLA
DAPI
50μm
M
Ntg
Ppara cTG
Relative Il6 promoter occupancy
IP:
PPARα
RelA

Figure 4. PPARα induces *Il6*. (A) Consensus sequences of PPRE and NFκB binding element. (B) Schematic representation of mouse *Il6* promoter. (C) The PPRE DNA sequences used in this study. (D) PPARα binds to the DR3 and κB element in the *Il6* promoter *in vitro*. Data shown are from a single experiment. However, key binding features, including stronger binding to the consensus PPRE than to the *Il6* κB element or its mutant, were reproducibly observed in at least two independent experiments (e.g., Fig. 5G) (E) PPARα mediates the *Il6* induction response to palmitic acid (PA). N=4. The immunoblot shown is representative of three independent experiments. (F) PPARα activators activate *Il6* transcription through the 1 Kb and 0.6 Kb *Il6* promoters.. N=6-8. (G) Fatty acid-induced *Il6* promoter activation is inhibited by dominant negative PPARα (PPARαΔAF2). N=8. (H) PPARα mediates PA- and WY-induced *Il6* promoter activation. N=6-8. (I) PPARα is recruited to the *Il6* promoter. N=5-6. (J) PPARα has an equivalent affinity for the κB element in the *Il6* promoter and PPREs in the *Cd36* and *Acox1* promoters. Data are representative of two independent experiments. (K) PA-, WY- and PPARα-induced *Il6* promoter activation is inhibited by a super suppressor form of IκBα. N=6-7. (L) PLA assay shows the binding of PPARα to NFκB. (M) PPARα and RelA bind to the *Il6* promoter. N=4-6. Statistical significance was assessed using the Kruskal–Wallis test for the 1 kb promoter stimulated with OA and the 0.6 kb promoter stimulated by *Ppara* overexpression in (F), and for PA stimulation in (K); the Mann–Whitney U test for PA stimulation in (H); Student's t-test in (M); and ANOVA for all other comparisons.

Figure 5

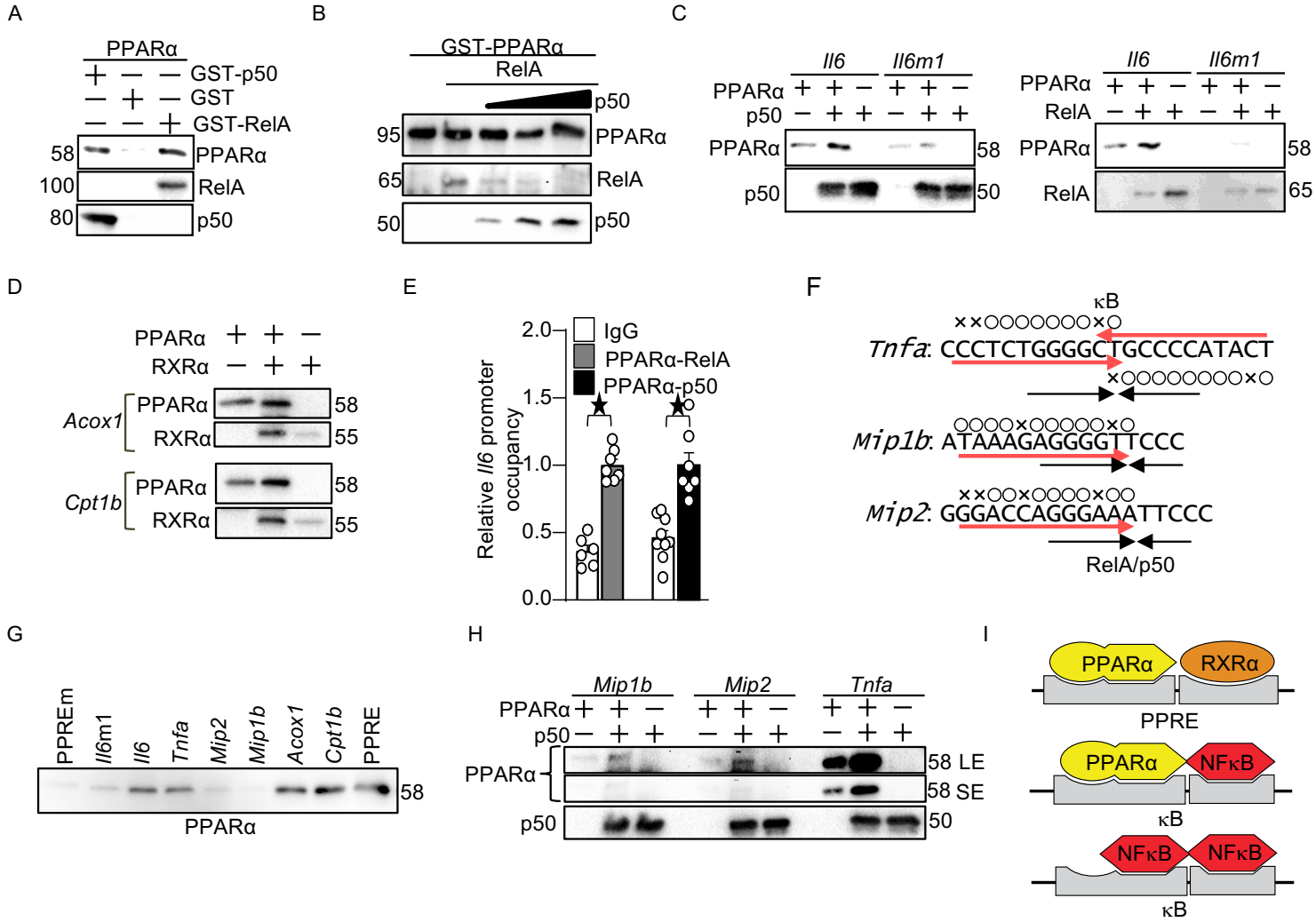
A
PPARα
GST-p50
GST
GST-RelA
58
PPARα
100
RelA
80
p50
B
GST-PPARα
RelA
p50
95
PPARα
65
RelA
50
p50
C
Il6
Il6m1
PPARα
p50
PPARα
58
p50
50
Il6
Il6m1
PPARα
RelA
PPARα
58
RelA
65
D
PPARα
RXRα
Acox1
PPARα
58
RXRα
55
Cpt1b
PPARα
58
RXRα
55
E
IgG
PPARα-RelA
PPARα-p50
Relative Il6 promoter occupancy
2.0
1.5
1.0
0.5
0.0
F
κB
Tnfa: CCCTCTGGGGCTGCCCCATACT
Mip1b: ATAAAGAGGGGTTCCC
Mip2: GGGACCAGGGAAATTCCC
RelA/p50
G
PPREm
Il6m1
Il6
Tnfa
Mip2
Mip1b
Acox1
Cpt1b
PPRE
58
PPARα
H
Mip1b
Mip2
Tnfa
PPARα
p50
PPARα
58 LE
58 SE
p50
50
I
PPARα
RXRα
PPRE
PPARα
NFκB
κB
NFκB
NFκB
κB
J
Il6
Mip1b
Mip2
Tnfa
PPARα
RelA
p50
ND
HFD
0.7
0.8
1.2
0.5
DR3
κB
0.5 Kbp

Figure 5. PPARα forms a heterodimer with NFκB. (A) PPARα directly binds to RelA and p50 *in vitro*. Data shown are from a single experiment; the interaction was independently examined using a reciprocal assay in Fig. 5B. (B) PPARα binds to NFκB proteins as a heterodimer entity. (C) The binding of PPARα to the κB element is enhanced by NFκB proteins. Each panel represents an independent immunoblot derived from a separate membrane. (D) The binding of PPARα to the PPRE is enhanced by RXRα. Data shown are from a single experiment. (E) PPARα and NFκB co-localize to the *Il6* promoter. Double ChIP assays were performed with the indicated antibodies and mouse hearts. N=6-9. (F) The endogenous κB sequences in *Tnfa, Mip1b-* and *Mip2* promoters. (G) PPARα binds to a subset of, but not all, endogenous κB elements. (H) The binding of PPARα to the κB element is enhanced by NFκB proteins. Data shown are from a single experiment; similar differential binding of PPARα to these elements was independently reproduced in Fig. 5G. (I) Schematic representation of PPARα binding to PPRE and κB element. (J) ChIP-seq shows that PPARα binds to the *Il6* and *Tnfa* promoters. The Y-axis in the UCSC genome browser is indicated at top right (0.5 - 1.2). ChIP-seq was performed once using pooled heart samples from three mice after one month of HFD feeding Data in (B), (C), and (G) are representative of two independent experiments. Statistical significance is indicated by a star and was assessed using Student's t-test (E).

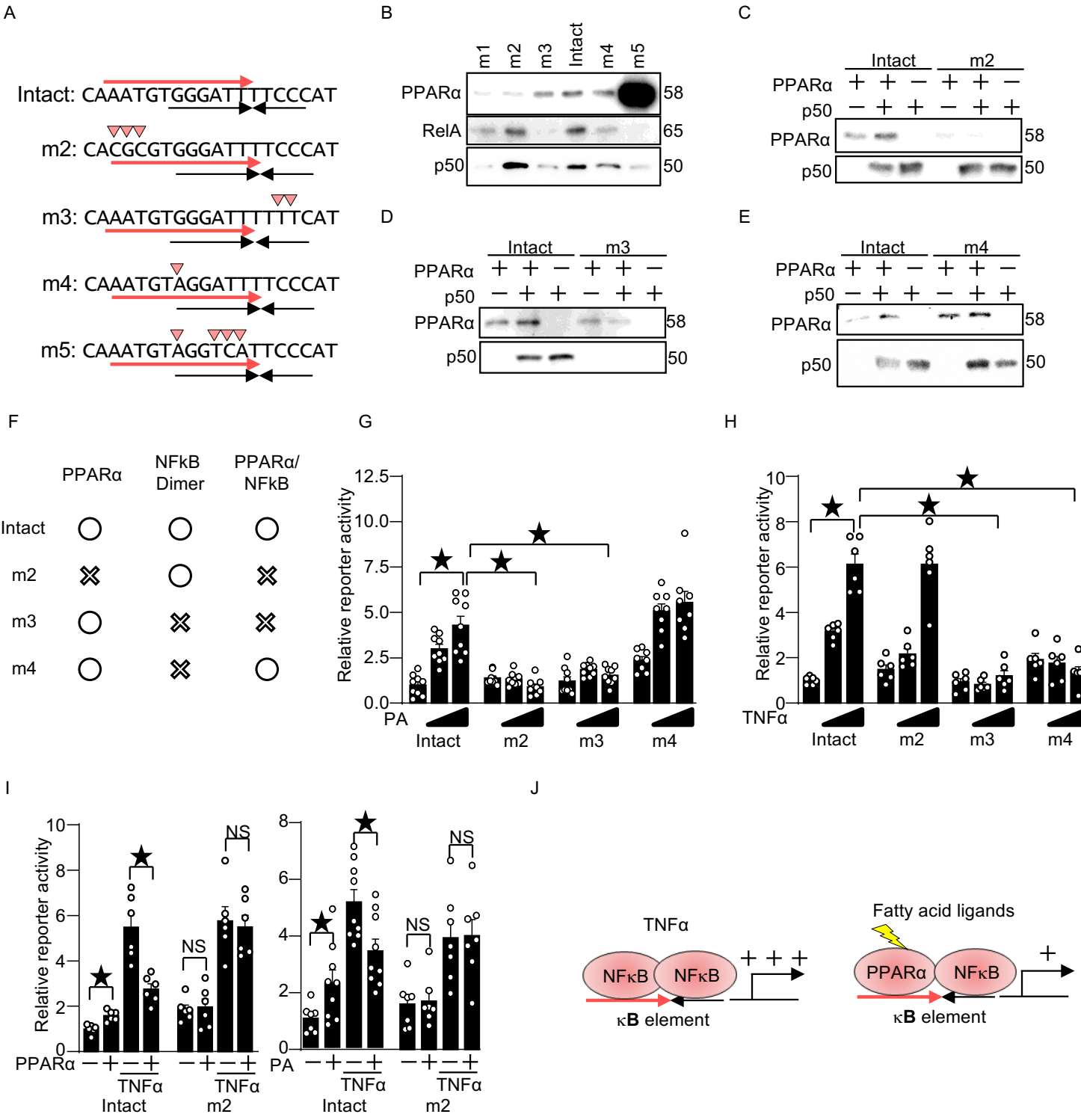
A
Intact: CAAATGTGGGATTTTCCCAT
m2: CACGCGTGGGATTTTCCCAT
m3: CAAATGTGGGATTTTTTCAT
m4: CAAATGTAGGATTTTCCCAT
m5: CAAATGTAGGTCATTCCCAT
B
m1 m2 m3 Intact m4 m5
PPARα 58
RelA 65
p50 50
C
Intact m2
PPARα + + − + + −
p50 − + + − + +
PPARα 58
p50 50
D
Intact m3
PPARα + + − + + −
p50 − + + − + +
PPARα 58
p50 50
E
Intact m4
PPARα + + − + + −
p50 − + + − + +
PPARα 58
p50 50
F
PPARα
NFkB Dimer
PPARα/ NFkB
Intact
m2
m3
m4
G
Relative reporter activity
12.5
10.0
7.5
5.0
2.5
0.0
PA
Intact m2 m3 m4
H
Relative reporter activity
10
8
6
4
2
0
TNFα
Intact m2 m3 m4
I
Relative reporter activity
PPARα − + − +
TNFα
Intact
m2
NS
PA
J
TNFα
NFκB NFκB
κB element
Fatty acid ligands
PPARα NFκB
κB element

Figure 6. PPARα/NFκB heterodimer is required for fatty acid-induced *Il6* promoter activation. (A) The κB element mutations used in this study. (B-E) *In vitro* DNA binding assays with the indicated recombinant proteins and mutated κB elements. Data in (B) are from a single experiment; the relative binding patterns observed in (B) were independently reproduced in (C)–(E), which are representative of at least two independent experiments. (F) Summary of PPARα and NFκB binding to the κB mutants. (G) PPARα/NFκB heterodimer is required for PA-induced *Il6* promoter activation. N=8-9. (H) PPARα is not required for TNFα-induced *Il6* promoter activation. N=6. (I) DNA binding of PPARα is required for fatty acid-induced *Il6* promoter activation and for inhibition of TNFα-induced *Il6* promoter activation. N=6-9. (J) Schematic representation of how TNFα-induced *Il6* promoter activation is mediated by NFκB dimer, whereas fatty acid-induced activation is mediated by PPARα/NFκB heterodimer. Statistical significance is indicated by a star and was assessed using ANOVA (G-H) and Student's t test (I).

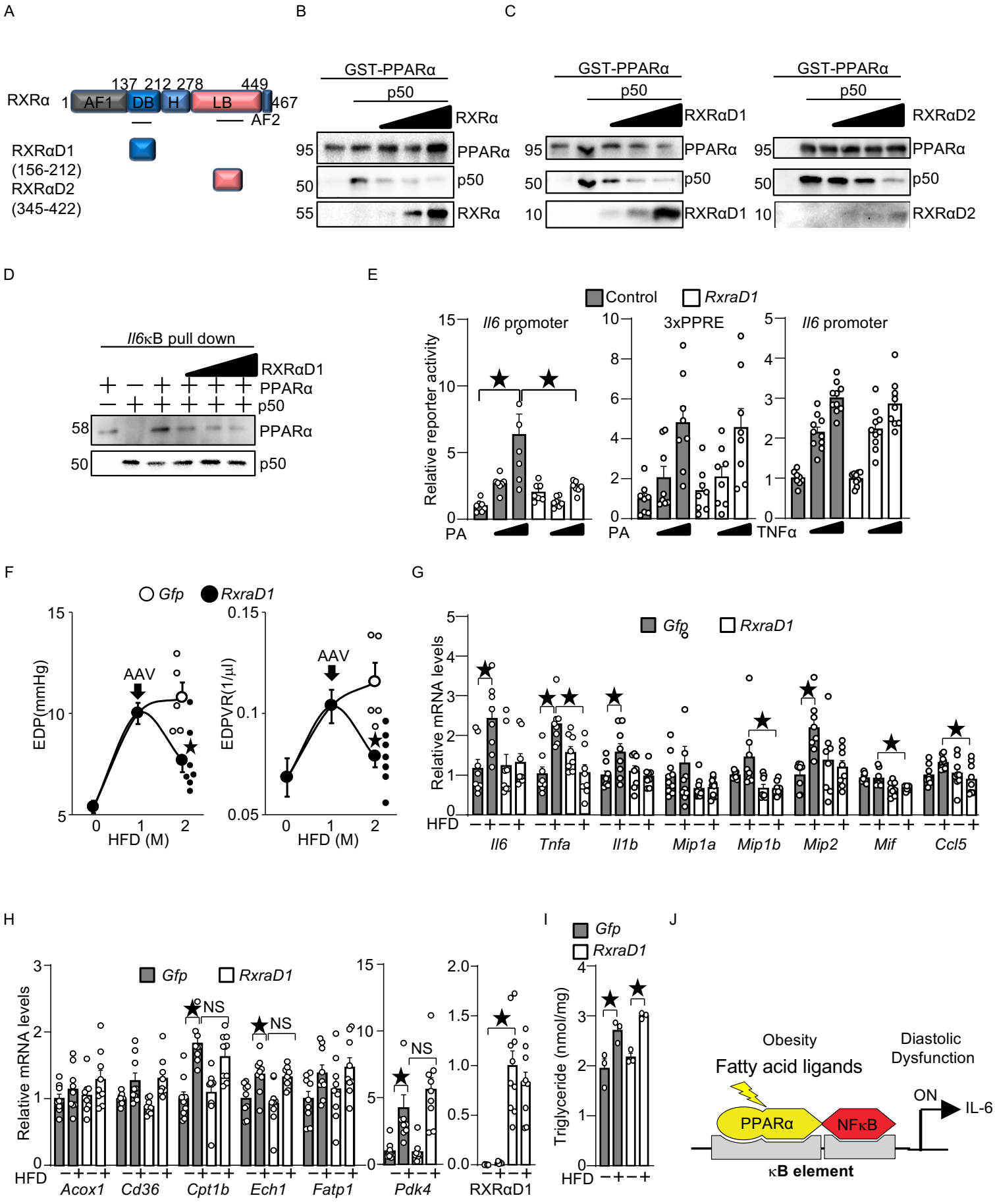
A
RXRα
137 212 278 449
1 AF1 DB H LB 467
AF2
RXRαD1
(156-212)
RXRαD2
(345-422)
B
GST-PPARα
p50
RXRα
95 PPARα
50 p50
55 RXRα
C
GST-PPARα
p50
RXRαD1
95 PPARα
50 p50
10 RXRαD1
GST-PPARα
p50
RXRαD2
95 PPARα
50 p50
10 RXRαD2
D
Il6κB pull down
RXRαD1
PPARα
p50
58 PPARα
50 p50
E
Control
RxraD1
Il6 promoter
3xPPRE
Il6 promoter
Relative reporter activity
PA
PA
TNFα
F
Gfp
RxraD1
EDP(mmHg)
AAV
HFD (M)
EDPVR(1/μl)
AAV
HFD (M)
G
Gfp
RxraD1
Relative mRNA levels
HFD
Il6
Tnfa
Il1b
Mip1a
Mip1b
Mip2
Mif
Ccl5
H
Gfp
RxraD1
Relative mRNA levels
NS
NS
NS
HFD
Acox1
Cd36
Cpt1b
Ech1
Fatp1
Pdk4
RXRαD1
I
Gfp
RxraD1
Triglyceride (nmol/mg)
HFD
J
Obesity
Fatty acid ligands
Diastolic
Dysfunction
PPARα
NFκB
ON
IL-6
κB element

Figure 7. PPARα/NFκB heterodimer mediates HFD-induced diastolic dysfunction. (A) Schematic representation of PPARα binding regions in RXRα. (B) Full length RXRα competitively inhibits the binding between PPARα and p50. (C) The DNA and ligand binding domains of RXRα competitively inhibit the binding between PPARα and p50. (D) RXRαD1 inhibits the binding of PPARα to the κB element but allows the binding of p50. Data in (B) and (C) were independently reproduced in three separate experiments, and data in (D) were independently reproduced in two separate experiments. (E) RXRαD1 specifically inhibits fatty acid-induced *Il6* promoter activation but not fatty acid-induced PPRE activation or TNFα-induced *Il6* promoter activation. N=7-10. (F) AAV-RXRαD1 ameliorates HFD-induced diastolic dysfunction. N=3-5. (G) AAV-RXRαD1 inhibits HFD-induced cytokine expression. N=8-10. (H) AAV-RXRαD1 does not affect authentic PPARα target gene expression. N=9. (I) AAV-RXRαD1 does not significantly affect triglyceride content in the heart. N=3. (J) Model of how PPARα contributes to diastolic dysfunction. Statistical significance is indicated by a star and was assessed using Student's t-test in (F); the Kruskal–Wallis test for *Il6, Tnfa,* and *Mip1b* in (G), and for *Cd36, Pdk4*, and *RxraD1* in (H); and ANOVA for all other comparisons.